

# Measured and modelled air quality related effects of a noise barrier near a busy highway

Sami D. Harni<sup>1</sup>, Lasse Johansson<sup>1</sup>, Jarkko V. Niemi<sup>2</sup>, Ville Silvonen<sup>3</sup>, Juan Andrés Casquero-Vera<sup>4,5</sup>, Anu Kousa<sup>2</sup>, Krista Luoma<sup>1</sup>, Viet Le<sup>1</sup>, David Brus<sup>1</sup>, Konstantinos Doulgeris<sup>1</sup>, Topi Rönkkö<sup>3</sup>, Hanna E. Manninen<sup>2</sup>, Tuukka Petäjä<sup>4</sup>, and Hilikka Timonen<sup>1</sup>

<sup>1</sup>Atmospheric Composition Research, Finnish Meteorological Institute, PL 503, FIN-00101 Helsinki, Finland

<sup>2</sup>Helsinki Region Environmental Services Authority HSY, Helsinki, Finland

<sup>3</sup>Aerosol Physics Laboratory, Physics Unit, Faculty of Engineering and Natural Sciences Tampere University, Korkeakoulunkatu 3, 33720 Tampere, Finland

<sup>4</sup>Institute for Atmospheric and Earth System Research, Faculty of Science, University of Helsinki, Helsinki 00014, Finland

<sup>5</sup>Andalusian Institute for Earth System Research, IISTA-CEAMA, University of Granada, Junta de Andalucía, Granada, 18006, Spain

*Correspondence to:* Sami Harni (sami.harni@fmi.fi)

**Abstract.** A three-month air quality measurement campaign was conducted in spring 2023 near a busy highway in Espoo, Finland. The measurement site featured a high (6.5 m) noise barrier built adjacent to the highway. Additionally, there was a gap in the noise barrier at the selected measurement site, providing an opportunity to study the air quality impacts of the noise barrier. Several air quality measurement devices were installed behind the noise barrier and in the gap at distances of 10, 20 and 40 m from the side of the highway. Additionally, 15 passive samplers were deployed to monitor NO<sub>2</sub> concentrations across the study area, mobile measurements were conducted using the ATMo-Lab mobile laboratory on the highway, and concurrent flights with drones equipped with AQ monitors were performed along the highway.

The effects of the noise barrier on PM<sub>10</sub>, PM<sub>2.5</sub>, lung deposited surface area (LDSA), particle number concentration (PNC), NO<sub>2</sub>, and black carbon (BC) were quantified based on the analysed measurement data. Furthermore, the measurements were compared with simulated pollutant concentrations from a local-scale Gaussian air quality model (Enfuser) with a nearby obstacle detection and concentration reduction method incorporated in the model to address the effects of the noise barrier in the study.

The noise barrier was found to effectively reduce pollutant concentrations behind the barrier. The most notable reductions were observed closest to the highway. The greatest reductions were observed for PM<sub>10</sub> (mostly road dust) while gaseous concentrations, such as NO<sub>2</sub>, exhibited less pronounced decreases.

## 1 Introduction

Traffic strongly influences air quality near highways through both exhaust emissions (Hilker et al., 2019; Sofowote et al., 2018) and wearing products originating from pavement, tyres and brakes as well as NaCl from winter salting (Denby et al.,

2016; Kupiainen et al., 2016; Pirjola et al., 2010; Sofowote et al., 2018; Vouitsis et al., 2023). These emissions pose risks to both human health and climate (Baensch-Baltruschat et al., 2020; WHO, 2021). The composition and size of particulate emissions from traffic vary, largely depending on the source. Combustion processes produce vast amounts of black carbon and organic-containing nanoparticles (Rönkkö & Timonen, 2019). The non-exhaust particles from traffic tend to be in the coarse mode size range and contain a mix of organics, metallic trace elements and NaCl from road salting (Denby et al., 2016; Vouitsis et al., 2023). Advancements in exhaust after-treatment technologies have been highly effective in reducing particulate emissions from traffic (Gren et al., 2021). These systems, combined with the increasing electrification of vehicles, have already led to a large reduction in exhaust-related emissions. Current EU legislations on particle emissions from traffic exhaust are so stringent that, in some jurisdictions, non-exhaust particles now represent a larger share of traffic-related particulate matter emissions (Fussell et al., 2022). In Europe, the upcoming Euro 7 legislation will also regulate tyre and brake wear emissions. The worldwide interest in reducing atmospheric pollutants is of great importance. This is reflected by the WHO air quality guidelines that include pollutants such as PM<sub>2.5</sub>, PM<sub>10</sub>, O<sub>3</sub>, NO<sub>2</sub>, SO<sub>2</sub> and CO. However, ultrafine particle number concentration (PNC) and elemental carbon (EC) are also included in good practice statements and systematic measurements of them are encouraged (WHO, 2021). Also, much stricter limits for various pollutants are going to be implemented with the new EU air quality directive, with an obligation to measure ultrafine particle (UFP) and black carbon (BC) concentrations (European Air Quality Directive, 2024).

Distance from the road has been found to strongly affect pollutant concentrations, with notable decreasing gradients observed for NO and NO<sub>2</sub> as distance increases from roads (Thoma et al., 2008). Pollutant concentrations perpendicular to highways have been found to follow logarithmic gradients, with the steepest decrease occurring near the road (Zheng et al., 2022).. Similarly shaped gradients of pollutant concentration on the side of the highway have also been observed as a function of time after being emitted on the road (Kangasniemi et al., 2019). The gradients for particles are found to be more pronounced for larger particles (Zheng et al., 2022). In an earlier study, noise barriers have been found to reduce NO<sub>x</sub> concentrations by 23 % at 5 m behind the noise barrier (Tezel-Oguz et al., 2023). Notably lower concentrations have been observed for traffic-related ultrafine particles, BC, CO and NO<sub>2</sub> concentrations behind the noise barrier compared to areas with no noise barrier, even at 300 m behind the noise barrier by Baldauf et al. (2016). The steepness of the pollutant gradient has been found to be strongly dependent on the flow dynamics (Enroth et al., 2016). This would suggest that noise barriers strongly affect the dispersion of pollutants on the roadside. The beneficial effects of noise barriers on air quality have also been reported by Li et al. (2021).

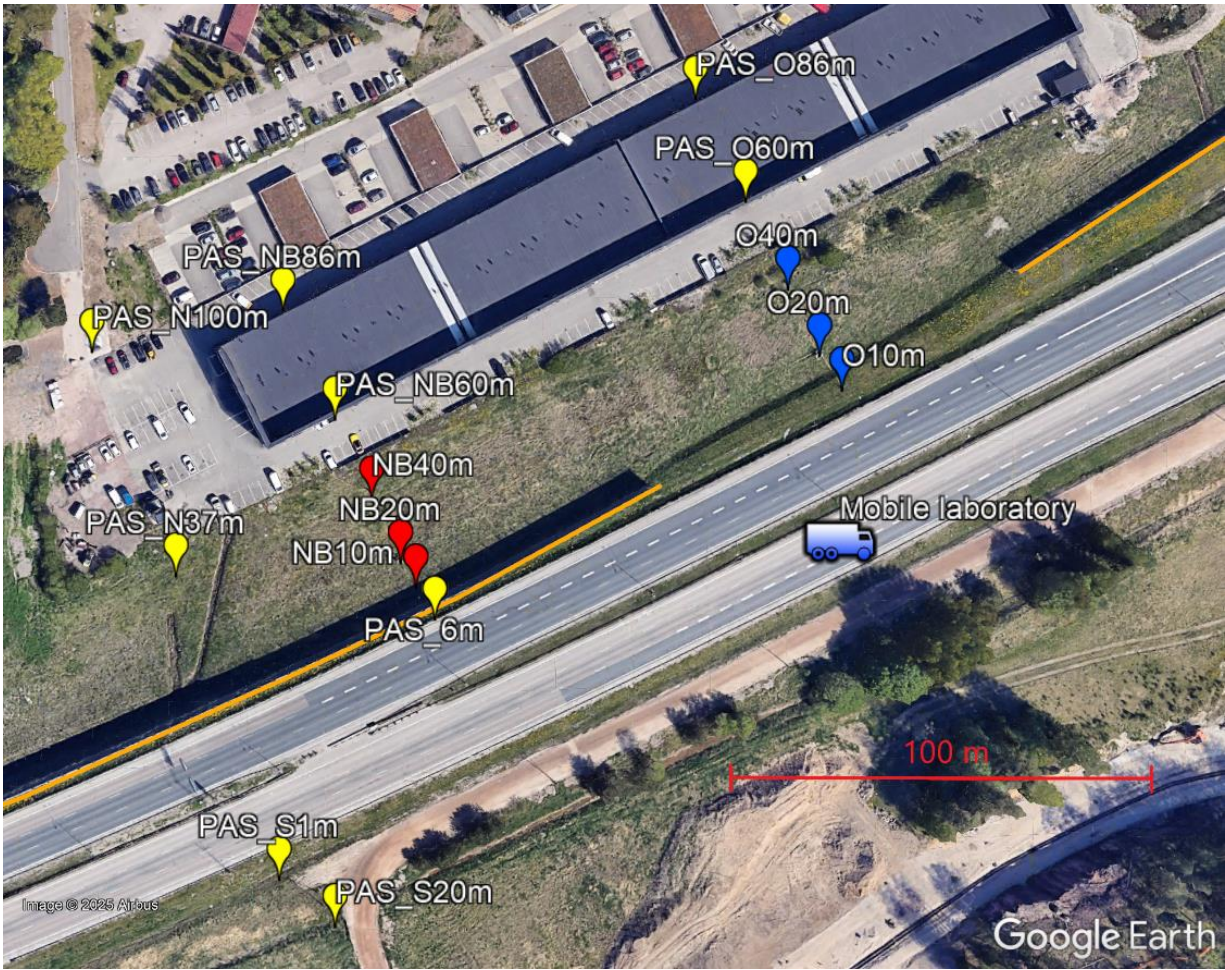
Several modelling approaches have been developed to meet the demand for accurate and timely information on urban AQ (Johansson et al., 2022; Rolstad Denby et al., 2020). The spatial variability of pollutant concentrations within an urban environment is pronounced, which poses a challenge for air quality modelling systems. To facilitate operational, timely production, the urban-scale models are mostly Gaussian dispersion models. However, the proper modelling of fluid dynamics in a complex environment would need more sophisticated tools such as Lagrangian particle simulations or Large Eddy Simulations (LES) (Hellsten et al., 2021). Unfortunately, the computational cost of using such sophisticated tools makes the

65 adoption of such approaches infeasible when the assessment time period exceeds several days, or the modelling area fully covers a city.

The objectives of this study can be summarised to: what is the effect of the noise barriers on the pollutant gradients and concentrations on the side of a highly trafficked highway, and how do the modelling results compare to the measurements? More specifically, this study aimed to characterise the influence of a noise barrier on air quality near a highway using a sensor  
70 type and mobile measurement platforms. Sensors were used to measure  $PM_{10}$ ,  $PM_{2.5}$ ,  $NO_2$ , BC, LDSA and  $NO_2$  concentrations as a function of distance (10, 20 and 40 m) from the highway, both behind a noise barrier and in an open area. PNC was also measured using sensor measurement, but only at 20 and 40 m poles. In addition, two condensation particle counters (CPCs) were used to study PNCs at the 20 m distances. Mobile measurements were conducted on the adjacent highway with the mobile laboratory. Additionally, fifteen passive samplers were deployed to monitor  $NO_2$  concentrations around the measurement  
75 location.

Another aim of this study was to test the capability of a Gaussian urban-scale dispersion model to quantify the effects of urban obstacles such as noise barriers while using computationally lightweight methods, which are feasible for operational use. The data included here provides urgently needed information about the influence of noise barriers and can be used to make better annual air quality maps for roadside locations for city planners.

2.1 Measurement campaign location and infrastructure



85 **Figure 1: Measurement infrastructure at the measurement site. The noise barrier has been marked to figure with orange lines. The measurement poles behind the noise barrier (NB10m, NB20m, and NB40m) have been marked with red, and the measurement poles in the open area (O10m, O20m, and O40m) have been marked with blue. Passive NO<sub>2</sub> samplers (PAS\_N100m, PAS\_N37m, PAS\_S1m, PAS\_S20m, PAS\_6m, PAS\_NB60m, PAS\_NB86m, PAS\_O60m and PAS\_O86m) have been marked in yellow. There were also passive samplers located in the main measurement poles. Also, a mobile laboratory is presented in the figure. (© Google Earth 2024)**

90 Measurements were conducted from March 1<sup>st</sup> to May 31<sup>st</sup> of 2023 near a busy highway (60°12'10.7"N, 24°44'14.1"E) that connects two major cities (Helsinki and Turku) in Southern Finland. According to (DigiTraffic, 2024), the daily traffic flow at the highway was approximately 63,000 vehicles/working day with an average speed of 85 km/h. The share of heavy-duty vehicles was approximately 5% during working days (Monday to Friday). The measurement site was located between a warehouse and the highway (Fig. 1). Next to the highway, approximately 7 m from the highway, a 6.5 m high noise barrier

had been built. Additionally, there was a 100 m gap in the noise barrier in front of the warehouse. The area around the measurement poles between the noise barrier and the warehouse was flat with only grass and no obstacles, including trees that could have affected the dispersion of pollutants.

## 2.2 Fixed instrumentation at the campaign site

Two rows of measurement poles were installed at distances of 10, 20 and 40 m from the highway (Fig. 1). One row of sensors was situated behind the noise barrier (poles named NB10m, NB20m, NB40m) while the other row was placed in the open area (O10m, O20m, O40m). The measuring height of the air quality sensors was about 2 m. In addition to the measurement poles, 15 NO<sub>2</sub> passive samplers were set around the measurement location. Six of the passive samplers were located at the measurement poles, and the other 9 in locations seen in Fig. 1. The passive samplers were measuring from February to May. The results were calculated monthly, but the March data were excluded because of data quality issues.

Following air quality parameters related to street dust and exhaust gases were measured: PM<sub>10</sub> and PM<sub>2.5</sub> (particle mass with diameter < 10 or 2.5 μm, Vaisala model AQT530, Note: AQT530 Vaisala measured particle size > 0.6 μm, Petäjä et al. (2021)), NO<sub>2</sub> (AQT530, Vaisala; IVL type passive samplers), black carbon (BC; AE51, AethLabs; ObservAir, DSTech), particle number concentration (PNC, AQ Urban, Pegasor) and lung deposited surface area (LDSA; AQ Urban, Pegasor; Partector, Naneos). Vaisala AQT530 sensor is described by Petäjä et al. (2021), Pegasor AQ Urban by Kuula et al. (2020), BC sensors by Chen & Lin (2013) (AE51) and Caubel et al. (2019) (ObservAir). IVL-type passive sampler for NO<sub>2</sub> is described by Ferm (1991) and Ayers et al. (1998). Two CPCs, Airmodus A30 (modified by the manufacturer to the 7 nm cut size; Airmodus Ltd., Helsinki, Finland – briefly described in Wlasits et al., 2024) and Brechtel 1720 (Brechtel Manufacturing, 258 Hayward, USA – described in BMI, 2021) were used to measure total particle number concentrations for particles larger than 7 nm at poles O20m and NB20m, respectively. However, these additional measurements fall out of the scope of this work and can be used as data input in future studies. Before and after the highway campaign, the air quality sensors were tested in co-location measurements with reference instruments at air quality monitoring stations. In the colocation measurements, the BC sensors were compared to MAAP. The average deviation from the MAAP was calculated, and the measurement data was corrected by multiplying the data by the derived correction factor. A similar process was also used for LDSA sensors (Partector) to make the concentrations to the same level between the instruments. Additionally, Partector sensors were also made comparable to AQ Urban by multiplying the LDSA concentrations by 0.66.

Data coverages of data usable in analysis for the different instruments are presented in the supplemental materials Table S1. For NO<sub>2</sub>, only the data from March was used as the authors wanted to be sure that all 6 instruments were functioning properly at the same time, and during April and May, the weather got warmer, and the measurement data seemed to include more errors and was therefore left out of the analysis. Also, the BC data from April and March was removed from the analysis as the large,

125 fast temperature changes between day and night caused artefacts in the data. The temperature-related issues of BC sensors are well described by Elomaa et al. (2024).

**2.3 Weather conditions during the measurement campaign**

130 The weather conditions, including hourly temperature, boundary layer height, precipitation, and water on the road, are presented in Fig. 2. During the measurement campaign, the meteorological conditions changed from winter conditions with subzero temperatures (minimum hourly temperature -10°C.) to spring with temperatures up to +20°C. The precipitation (mostly snow) was quite frequent in March, whereas only some precipitation (mostly rain) was observed in April and May. Especially the beginning of April was distinctively dry. The presented weather conditions are a mix of measured and modelled information; the boundary layer height originates from the SILAM chemical transport model (CTM) (Sofiev et al., 2015), and 135 the water column height on the road surface is taken from the closest optical road weather measurement site (DigiTraffic, 2024).

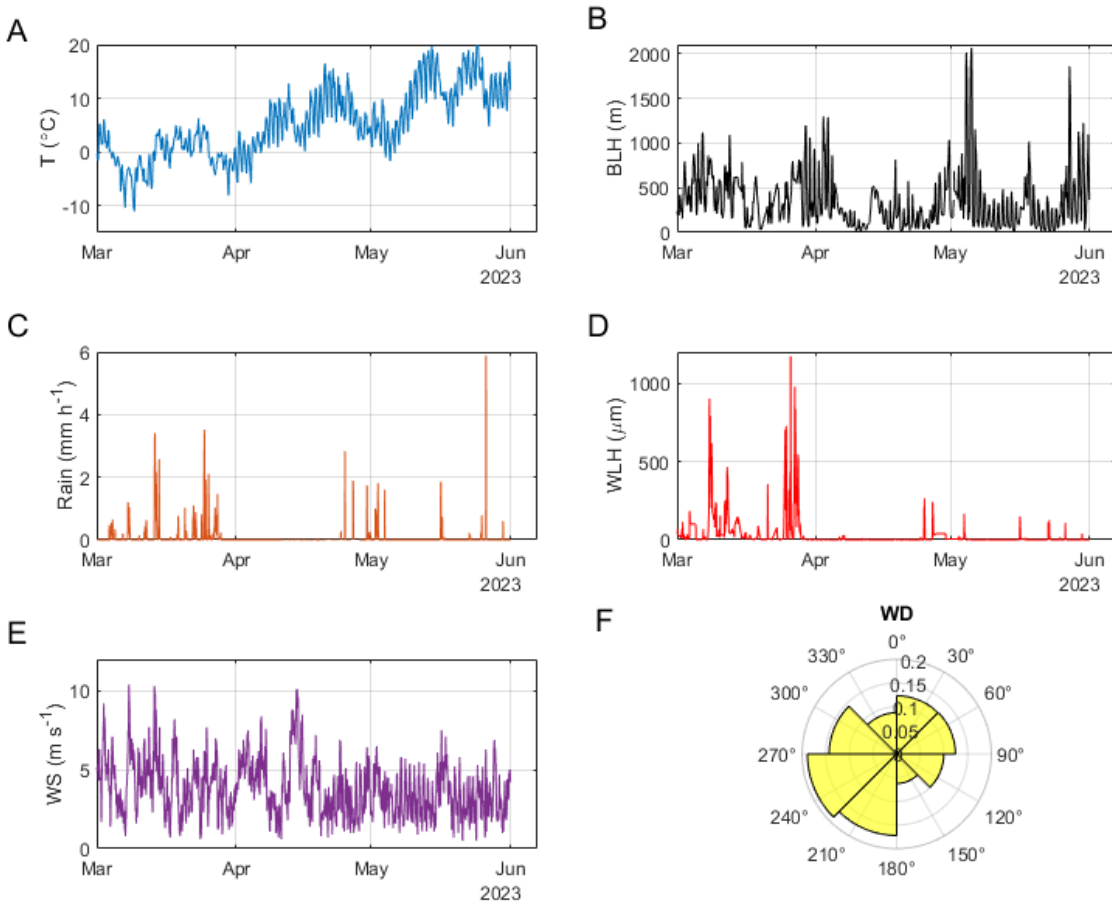


**Figure 2: The weather data including A) Temperature ( $T$ ), B) Boundary layer height (BLH), C) Rain, D) Water layer height on road (WLH), E) Wind speed (WS) and F) Wind direction (WD) during the measurement period (March 1<sup>st</sup> to May 31<sup>st</sup>, 2023).**

## 140 2.4 Mobile and drone measurements

Mobile measurements on the highway were conducted using the ATMo-Lab mobile laboratory (Lepistö et al., 2023; Rönkkö et al., 2017). The air was sampled from the top of the windshield at a height of  $\sim 2.2$  m with a flow rate of 22 lpm. An 8 km loop was driven on two measurement days (Monday, 20<sup>th</sup> March and Friday, 24<sup>th</sup> March) between 11 am and 3 pm, resulting in 300 minutes of highway measurement data. Total particle number concentrations were measured with four CPCs with different D50 % cut diameters: 2.5 nm (TSI 3756), 4 nm (TSI 3775), 10 nm (Airmodus A20) and 22 nm (Airmodus A23). The size distribution of particles was measured with an electrical low-pressure impactor (Dekati ELPI+). Additionally, black carbon mass concentration (Magee Scientific AE33), particle chemical composition (Aerodyne Research Inc, soot-particle aerosol mass spectrometer; SP-AMS), CO<sub>2</sub>-concentration (LI-COR LI-850) and NO<sub>x</sub>-concentration (Teledyne T-201) were measured.

Of the measured components, the NO<sub>2</sub>, LDSA, PNC, and BC are compared to the stationary measurements in this paper by  
150 using the concentrations measured with the mobile laboratory as a reference point on the road.

Drone measurements were conducted with a custom-built multicopter built around the Tarot X6 hexacopter platform. The  
copter had a maximum flight time of 15 min. The maximum take-off weight for the copter was around 11 kg. During flight,  
the GPS locations and altitudes of the copter were recorded using (GPS – Global Positioning System – position fix). The  
155 scientific instrumentation was attached to purpose-built modules. The exact description of the drone is given by Brus et al.  
(2021). The scientific payload of the drone consisted of condensational particle counters (CPCs; model 3007, TSI Corp.; total  
count in the range from 0.01 to >1.0 µm), the mini cloud droplet analyser (mCDA, Palas GmbH) with a size range of 0.2-17  
µm in 256 bins resolution), a micro Aethalometer (model MA200, microAeth), a basic meteorological sensor  
(Bosch BME280; P, pressure; T, temperature; and RH, relative humidity), and Raspberry 4 microcomputer. The data from the  
160 instruments were recorded on the microcomputer with a 1 Hz resolution. The drone measurements are used in this paper for  
evaluating the vertical dispersion of pollutants.

## 2.4 Modelling framework

Enfuser is an urban-scale air quality model (Johansson et al., 2022). The modelling approach for local emission sources is  
Gaussian (a combination of Gaussian plume and puff methodologies), and long-range transportation of pollutants is addressed  
165 by incorporating a regional-scale AQ forecast to define hourly background concentrations. As a novelty, the model uses AQ  
measurement-driven data assimilation to adjust these background concentrations, but also emission-source specific emission  
factors on an hourly basis.

Among other areas of interest, Enfuser is currently being used operationally in the Helsinki metropolitan area in Finland. The  
170 outputs of the model are hourly average pollutant concentrations (e.g., PM<sub>2.5</sub>, PM<sub>10</sub>, NO<sub>2</sub>, O<sub>3</sub>, PNC, BC and LDSA) at a  
breathing height of 2 m above ground, and this output provided is publicly available via FMI's Open Data portal (FMI, 2024).  
The modelling resolution in the Helsinki region is 13 x 13m<sup>2</sup>, with circa two million receptor points (grid cells). In addition,  
hourly updating air quality index (AQI) visualisations based on the model results are available at (HSY, 2024). The key  
emission sources being modelled include road traffic emissions (also resuspension of particles), residential wood combustion,  
175 marine shipping, and local power plants.

Details on the Enfuser modelling system and its input sources in the Helsinki metropolitan area have been presented in  
(Johansson et al., 2022). In summary, the most essential information sources are as follows:

- HARMONIE numerical weather prediction model (NWP) (Bengtsson et al., 2017) is used as the main source for  
meteorological input. In addition, the local road weather measurement network gives additional information on, e.g.,  
180 road surface moisture that impacts the modelling of PM<sub>10</sub>.



- The regional background is given by the SILAM CTM model (Sofiev et al., 2015).
- Online AQ measurement results are extracted from the FMI Open data portal. In addition, complementary sources for AQ data have been included to incorporate, e.g., AQ sensors that are maintained by local authorities.
- A wide range of heterogeneous GIS inputs is used and assimilated to characterise the modelling area and urban structures within the area. The most notable source in this regard is the OpenStreetMap (OSM).

The Enfuser model for the whole Helsinki metropolitan area is used to predict hourly pollutant concentrations from January 1<sup>st</sup> of 2023, up to 31<sup>st</sup> of May 2023. During the modelling, all available reference quality AQ measurement data is used in the model's data assimilation (Johansson et al, 2022). During the data assimilation, model predictions are iteratively being made at the exact measurement locations and heights, while the background levels and emission factors are gradually adjusted to obtain a better agreement between the predictions and the measurement evidence. This process occurs for each hour and for each modelled pollutant species separately. However, the modelling results for sensors used in this measurement campaign have all been excluded from this set of inputs to facilitate an unbiased comparison against model predictions.

In addition to the modelled concentration fields for the Helsinki metropolitan area, the model is used to assess high-resolution concentration predictions with a 4x4 m<sup>2</sup> grid around the measurement campaign area for the duration of the campaign. The modelling duration prior to this can be regarded as a spin-up period for data assimilation methods adopted in the model. Finally, the modelled concentrations are compared against the measured hourly concentrations for all sensors. In this comparison, the model is used to predict the concentrations using the exact coordinates and listed measurement heights for all the sensors, as opposed to fetching the model predictions from the raster output with predefined resolution.

#### **2.4.1 Modelling the effects of the noise barrier**

The Enfuser model uses various geographic information sources to describe the modelling area and its characteristics, including buildings (and their heights) and other urban ,landscape properties via OSM. The overall topography is given by NASA SRTM. These geographic sources of information, and several others, have been pre-processed into a high-resolution 2D datasets (4 x 4 m<sup>2</sup>) prior the use of the model (Johansson et al., 2022). The preprocessing of the geographic datasets facilitates faster computations via, e.g., fast building and obstacle detections around the receptor locations. The building height information is based on OSM if the height property or floor count for the object has been specified; otherwise, an approximated building height value is obtained from Global Human Settlement (GHS-BUILT-H R2023A).

The vicinity of urban structures and their impact on the dispersion of pollutants can be addressed in a simplified manner, considering the limitations of Gaussian dispersion modelling techniques. The approach has been illustrated in Fig. 3. For any given location of interest (referred to as a receptor point, RP) for which model predictions are made, the surrounding area is first scanned to detect urban obstacles. This scanning is done in 10-degree sectors up to 125 m. In case an obstacle is detected,

the angle of observation and the height of the object are logged. In case there are multiple obstacles with varying heights, the obstacle with a higher angle of observation takes priority.

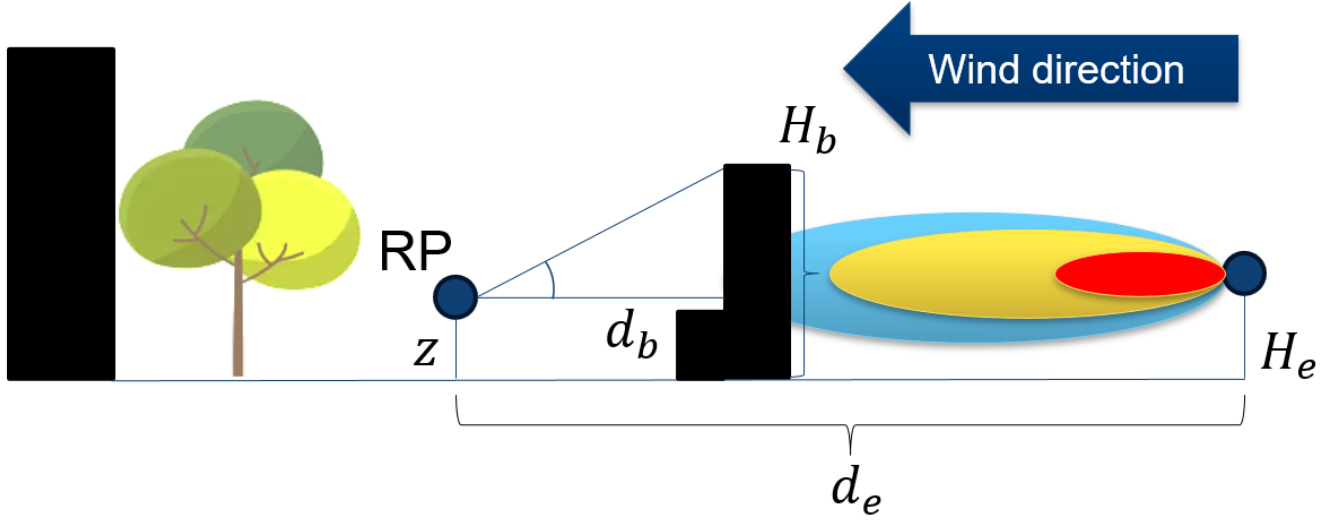


**Figure 3: Illustration of the modelling approach and known distance and height measures for reducing concentrations due to barriers.** A singular emission source at a distance of  $d_e$  is shown from a receptor point (RP) in which the concentrations are computed. Given the ambient wind direction, the precomputed distances to local barriers or buildings and their heights are fetched. In case an obstacle exists between the emitter and the RP, then the shown distance and height measures are used to apply a reduction for modelled Gaussian plume concentrations.

Let us consider an emission source (e) at some location near the RP for which the emission release rate [ $\mu\text{gs}^{-1}$ ] for a pollutant species is known. Depending on the measurement height  $z$ , the emission release height  $H_e$  and ambient wind conditions, the Gaussian steady-state solution can be used to estimate the concentrations at the point RP ( $c_{RP}$ ) caused by the emitter at RP while ignoring the effects of urban terrain (Seinfeld and Pandis, 2016). Using the precomputed (scanned) obstacle detection around RP, it can be assessed whether there are obstacles between the emitter and the RP. In case there is an obstacle at a distance of  $d_b$  with height  $H_b$  in between the two points, a reduction caused by the obstacle is approximated, as some fraction of the pollutants is physically unable to disperse to the RP and remains behind the object. The reduction effect should be more prominent the closer the emission source is to the obstacle. However, as can be seen from Fig. 3, this distance measure ( $d$ ) is not readily available (without costly, additional checks), and we approximate it to be  $d \approx d_e - d_b$ . Using a single hyperparameter ( $a$ ), we define an approximation of how the distance to the blocker reduces the concentration  $c_{RP}$  given by:

$R_d = 1 - ad, R_d \geq 0$	(1)
----------------------------	-----

where the hyperparameter  $a$  defines how sensitive the reduction is as a function of distance  $d$ . Simply put, with a low value of  $d$ , the  $R_d$  is close to 1 (almost full reduction) and conversely with a maximum distance value ( $d = a$ )  $R_d$  is equal to 0 (no reduction). The physical interpretation of Eq. 1 is that the emissions originating far behind the barrier can be considered well-mixed, and the effect of the barrier gradually and continuously loses relevance as a function of the distance.

In addition, we assume that the reduction is proportional to the elevation difference  $H = (H_b - H_e), H \geq 0$ . The strength of this effect is managed with another hyperparameter ( $b$ ) to estimate the reduction factor due to elevation difference, given by:

$$R_H = (H_b - H_e)b, R_H \in [0,1] \quad (2)$$

Finally, we can approximate the reduced concentration at RP,  $c'_{RP}$ , with

$$c'_{RP} \approx (1 - R_d R_H) c_{RP} \quad (3)$$

This simplistic reduction effect modelling (using as few parameters as possible) is applied with the noise barrier located within the measurement campaign site; the model is also applied to other obstacles, such as buildings, while acknowledging that the reduction model may not provide accurate results for such more complex objects. Noise barriers are described in OSM data, and it would be technically possible to automatically characterise them as obstacles for the model. Instead, in this study, we have manually inserted the noise barrier as a 6.5 m tall construct into the model inputs. In reality, the barrier is thin, but due to the way the object detection and the mapping of objects work in the model, the modelled barrier has an artificial width of 4 m (the minimum surface area of any object is 4x4 m).

In this study, we have used values  $a = 0.0033 \text{ m}^{-1}$  and  $b = 0.1 \text{ m}^{-1}$  for the hyperparameters. These hyperparameter values were obtained by using Monte Carlo simulation with the sensor data from NB10m, NB20m and NB40m, focusing on PNC,  $\text{PM}_{10}$  and LDSA measurements. The hyperparameters that minimised the root mean squared error over all the selected species were chosen. Presumably, the reduction effect is likely to be different for particles and gases, however, this possibility was not addressed to avoid the introduction of a third hyperparameter. Finally, in the special case the RP is located within a building (or an obstacle), the model ignores all nearby obstacles and applies a flat reduction factor (0.15) to all local emission contributions. The modelled concentration at the RP can then be regarded as an inaccurate placeholder value for indoor air quality (Fig. 13).

#### 2.4.2 Road traffic exhaust emission modelling

Road traffic emissions are modelled by combining hourly vehicle flow information for individual roads (given by OSM) coupled with vehicle class-specific emission factors. These emission factors are also flow-speed dependent, and the flow speed is also used to introduce instantaneous mixing due to the turbulence caused by the vehicles (Johansson et al., 2022). Individual roads are described as objects in the model with various characteristics. While these objects are not exactly lane-specific, the different flow directions are most often represented by separate and independent objects. For example, at the campaign site, the highway has two separate parallel road objects that characterise the traffic flows to the West and separately to the East (Fig. 4). Both objects characterise the number of lanes, but this information is only used in defining the width of the emission

source, assuming that the vehicle flows are evenly distributed to the lanes. In this study, the westbound section of the road, which is closer to the measurement campaign site, has a greater impact on the concentrations at the measurement locations.

In the Enfuser model, the average hourly flow counts are described for each road object separately using 24 average flow values for working days (Monday to Friday), another 24 values for Saturdays and finally 24 values for average Sundays. This characterisation with 72 values is defined separately for cars and heavy vehicles. Additional “regional” modifiers (targeting all road objects) are used to address weekly variations (e.g., summer holiday months. In this study, traffic count data from the nearest DigiTraffic (2024) record were used to refine the average flow information applied in modelling the site area. This localised fine-tuning of the vehicle flows was possible since there is a traffic count sensor very close to the campaign site. As can be seen from the figure, the hourly flows of vehicles to the West and East are clearly different (asymmetric) for cars during working days.

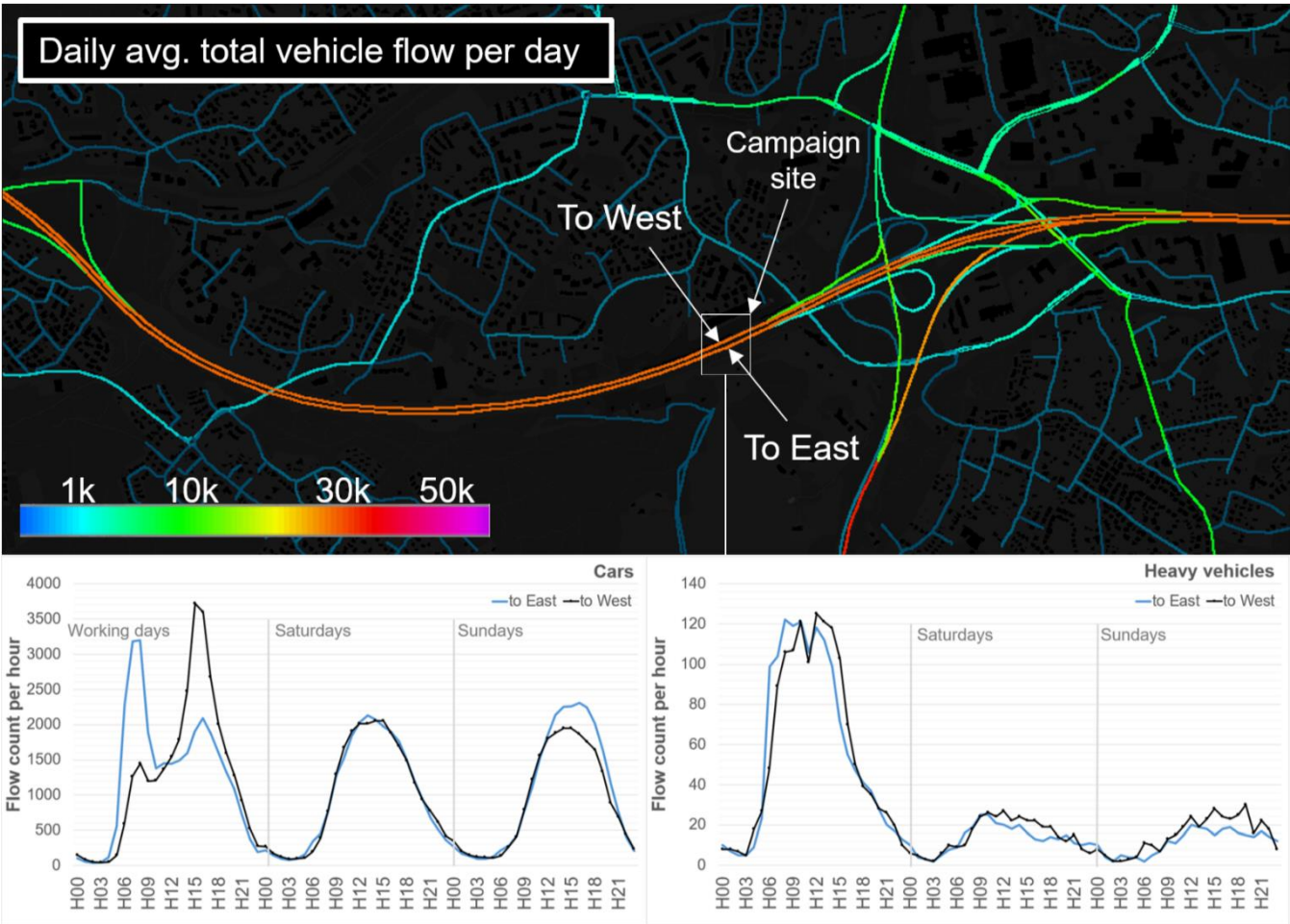


**Figure 4: Hourly average traffic flow information incorporated into the Enfuser model. Up, the overall daily average flows (cars) near the campaign site are shown. Below, the implemented direction-specific hourly traffic flows are shown**

280 **for cars and heavy vehicles in local time. The first 24-hourly flow counts correspond to working days (Monday to Friday), and the next 48 values correspond to Saturdays and Sundays.**

### **2.4.3 Modelling of non-exhaust emissions from road traffic**

The modelling of coarse particle generation (e.g., via the use of studded tyres) and resuspension of the particles is challenging; an overview of the approach has been presented in (Johansson et al., 2022). Recently, the use of machine learning-assisted  
285 modelling of road dust has also been investigated (Kassandros et al., 2023). Without relying on machine learning, however, the model describes a generic weekly pattern for the usage of studded tyres in the modelling area for passenger cars. This information, combined with the hourly flows of vehicles (while considering the flow speed), provides an upper limit function for the coarse particle fraction emissions. Further, we assume that heavy vehicles also generate coarse particles through wear and tear. This upper limit function is then limited (scaled down) based on road surface moisture. Simply put, for a road that is  
290 wet or covered in ice and snow, the upper limit function is reduced to near-zero values. As a complication, the Gaussian models struggle to consider dynamic phenomena such as the generation of resuspension particles in the past; based on our previous studies of diurnal variability of PM<sub>10</sub> concentrations in urban traffic monitoring stations we have learned to incorporate the vehicle flow information from the past two hours to obtain better agreement with modelled and measured concentrations and to make hourly PM<sub>10</sub> predictions less sensitive to the most recent vehicle flows nearby. Finally, the modelled resuspension  
295 component is being adjusted on an hourly basis according to the recent measurement evidence via the data assimilation routine. As described by Johansson et al. (2022), the data assimilation corrections cannot address local biases (e.g., an especially dusty road) but modify emission factors and background concentration across the whole modelling area.

### **2.4.4 LDSA, BC and PNC modelling**

300 In this study, we present results for LDSA, BC and PNC concentrations for the first time in Helsinki with the Enfuser model. The modelling approach for these new species is fairly similar to the modelling of, e.g., PM<sub>2.5</sub>, with a couple of exceptions. First, the emission factors are not well known for LDSA and PNC, and we rely on proxies that have been based on PM<sub>2.5</sub> emissions sources. Secondly, the SILAM CTM model does not provide regional background concentrations for LDSA or PNC, and thus, we again use a proxy based on SILAM PM<sub>2.5</sub> background. As these preliminary emission factors and background  
305 estimates are almost certainly biased, we rely on Enfuser's data assimilation method to gradually adjust these to the levels that provide the best fit against the measurement evidence. For example, we define an initial proxy factor for a given emission source sector (e.g., LDSA from residential sources is 6 times the emissions of PM<sub>2.5</sub>) and let this proxy factor gradually develop over time. The stabilisation of these freely floating emission factor parameters takes time, and this is one of the reasons the modelling time span has been set to begin on 1<sup>st</sup> of January. Finally, particle number concentrations are impacted by  
310 meteorological conditions, e.g., affecting coagulation (Gani et al., 2020). Since the measurement input for PNC (or LDSA) does not include size distributions, the modelling cannot address such effects.

### 3. Results and discussion

#### 3.1 Influence of the noise barrier based on measurement results

The influence of the noise barrier as a function of distance was analysed using the measurement data, for which the results are shown in this section. The gradients (i.e., concentration changes with distance) of the main pollutants PM<sub>10</sub> (> 0.6µm), PM<sub>2.5</sub> (> 0.6µm), PNC, LDSA, BC, and NO<sub>2</sub> are shown in Fig. 5. All measured pollutants show a clear decreasing gradient in the open area, with the largest decreases observed between O10m and O20m poles. The steepest gradients were observed for particulate-related pollutants PM<sub>10</sub> and PM<sub>2.5</sub>, which is in line with previous findings in the literature. For example, Zheng et al., (2022) found that larger particles have steeper and more pronounced roadside-decreasing gradients compared to smaller particles. The PM<sub>10</sub> and PM<sub>2.5</sub> gradients were likely to have been affected by the strong street dust season that enhanced the coarse particle concentrations on the highway compared to the background concentration. Additionally, the PM<sub>2.5</sub> gradient might have been slightly overestimated as the sensors measured only particle sizes > 0.6 µm and therefore the street dust contribution to PM<sub>2.5</sub> concentrations was exaggerated. The gradients of the large particles might also be due to the larger particles having slower dispersion, more efficient deposition and shorter removal times from the atmosphere compared to the gaseous pollutants and smaller particles (Kumar et al., 2008; Noll et al., 2001). The effect of noise barriers on NO<sub>2</sub> concentrations was less pronounced, and the effect of the noise barrier was diminished already at 20 m from the highway. Additionally, the decrease for PNC was notable despite measurements being available only at O20m and O40m poles (measurements from O10m were not available and likely would have shown the highest concentrations due to the proximity to the highway).

330

Behind the noise barrier, all the pollutant concentrations were lower when compared to the open area, with no clear decreasing gradients for the pollutants. Slight decreasing gradients even behind the noise barrier were detected for PNC, LDSA and NO<sub>2</sub>, but for PM<sub>10</sub> and PM<sub>2.5</sub>, there were no gradients behind the noise barrier, and the lowest concentrations were seen straight behind the noise barrier.

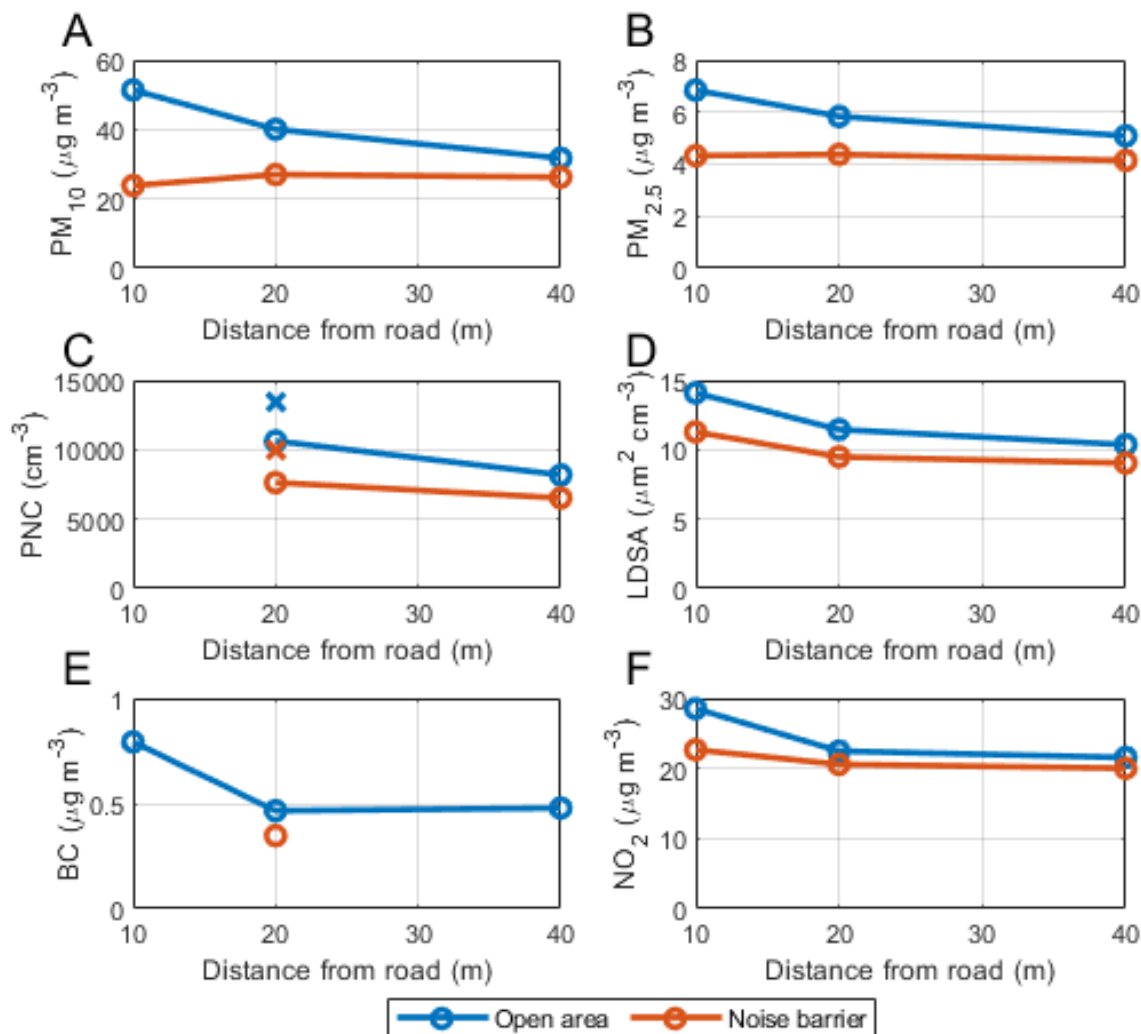
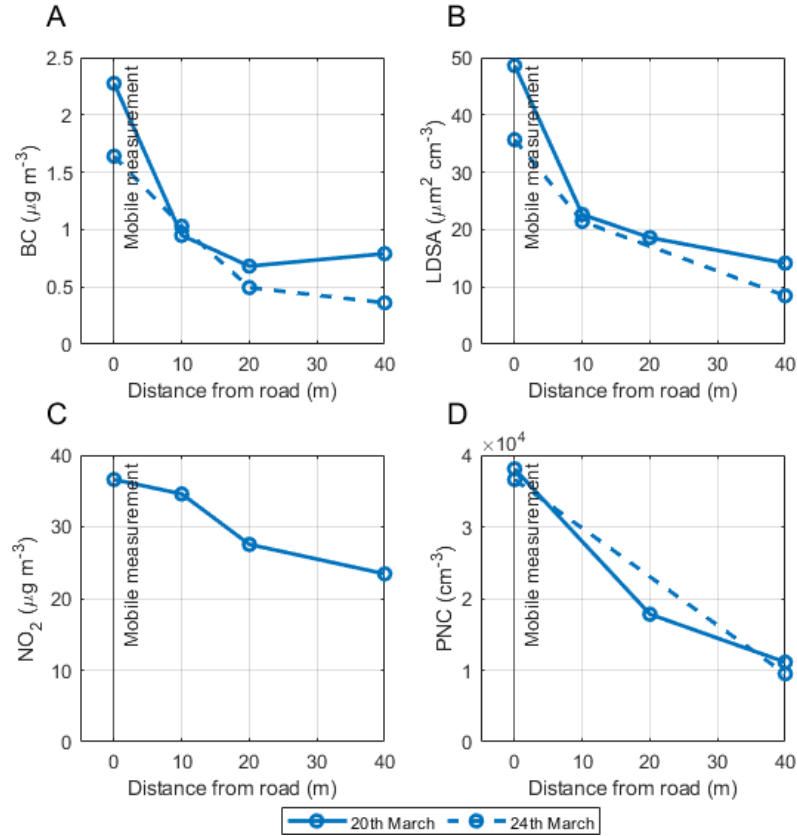


Figure 5: A) PM<sub>10</sub>, B) PM<sub>2.5</sub>, C) PNC, D) LDSA, E) BC, and F) NO<sub>2</sub> gradients in the open area and behind the noise barrier. In panel C, the PNC gradient has been measured with AQ urban sensors, and PNCs measured with CPCs have been presented with 'X'. IN panel E, the concentrations at 20 m have been measured with AE51 and concentrations at 10 and 40 m with ObservAir sensors. The gradients have been calculated over all the measured data. The data coverages for each parameter are presented in Supplement S1.

### 3.1.1 Characteristics of aerosol at the highway

During the measurement period, a mobile laboratory was used to measure pollutant concentrations on the highway for two days: March 20<sup>th</sup> between 12:45 and 14:50 and March 24<sup>th</sup> between 11:20 and 15:15 (local time). The corresponding stationary data for these hours were extracted and compared with the on-road measurements. Figure 6 represents the concentration gradients in the open area for BC, LDSA, NO<sub>2</sub> and PNC. BC data from all the poles were available during both measurement days. For both days, BC concentrations were higher on the highway compared to the roadside concentrations. On the roadside, the BC concentrations have a similar gradient to the one seen in Fig. 5, with concentrations decreasing steeply from 0 to 10 m to

O20m but either slightly decreasing (or even increasing) from O20m to O40m. For LDSA, data from the O20m pole on March 24<sup>th</sup> was missing. However, higher LDSA concentrations were observed on the highway compared to the roadside on both days. The gradients of LDSA and BC follow a logarithmic curve, consistent with earlier roadside observations by Enroth et al. (2016) and Zheng et al. (2022). Coincident stationary measurements of NO<sub>2</sub> were only available for March 20<sup>th</sup>. On this day, NO<sub>2</sub> concentration was only slightly higher on the highway compared to the O10m pole, with a steeper decrease between O10m and O20m. This trend may partly reflect the conversion of traffic-emitted NO to NO<sub>2</sub>, leaving a higher proportion of NO<sub>x</sub> as NO on the highway. In the case of Fig. 5, it was speculated that the decrease in PNC could be steeper closer to the highway if measurements were available. In Fig. 6, this seems to be the case as on the 20<sup>th</sup> of March, the decrease of PNC between the highway and O20m is greater compared to the decrease between O20m and O40m poles. On the 24<sup>th</sup> of March, the PNC data from the O20m pole was not available, however, the concentrations on the highway and at O40m were similar to those measured on the 20<sup>th</sup> of March.



**Figure 6: A) BC Gradient with mobile measurement. B) LDSA gradient with mobile measurement. C) NO<sub>2</sub> gradient with mobile measurement. D) PNC gradient with mobile measurement. The mobile measurement results have been added to the figure as 0 m points representing the side of the road.**



### 3.2 Drone measurements

Vertical differences in PNC at the site were studied with drone measurements. These measurements were performed at the same time as the mobile measurement. The PNC was measured using a multicopter, flying along the highway from behind the noise barrier to the open area at two different heights: 2 m and 15 m. In Figure 7, the results from these measurements are presented separately in two panels for the two measurement days, 20<sup>th</sup> and 24<sup>th</sup> of March. Each day includes four boxplots, corresponding to the heights of 2 m and 15 m, and with separate plots for the flight paths behind the noise barrier and in the open area. The measurement data nearer than 10 m the edge of the noise barrier were left out of the analysis, both in the open area and behind the noise barrier.

Figure 7 shows that the median concentrations, indicated by the red horizontal line in the figure, were slightly lower at a height of 15 m compared to 2 m on both days. The effect of the noise barrier on the concentrations measured with the drone seemed to be smaller compared to the measured gradient presented in Fig. 5. Also, the lowest concentrations were measured in an open area at an elevation of 15m, although the concentrations were only marginally lower. Notable was also the large variability of the PNC, with the measured values varying between a couple of thousands to more than 50,000 cm<sup>-3</sup> during both days, although the measurements only consisted of a total of 8 flights, 4 on each day. Each of the flights lasted for 5 to 10 minutes, and during both days. The pauses between flights were between 5 to 20 minutes.

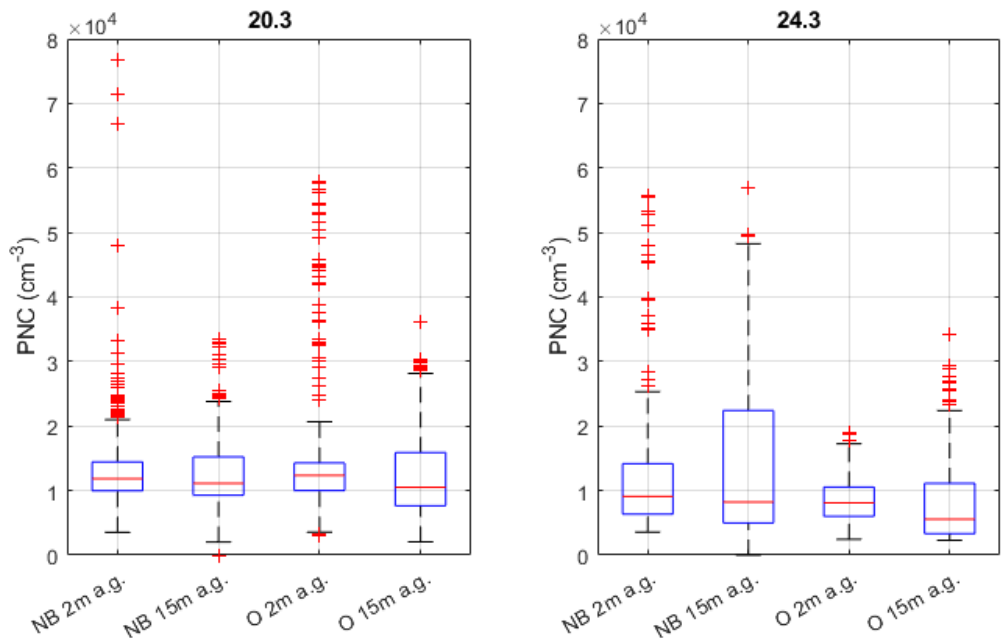


Figure 7: Boxplots of PNC measured with a drone in the open area (O 2m a.g., O 15m a.g.) and behind the noise barrier (NB 2m a.g., NB 15m a.g.) separately for the 20<sup>th</sup> and 24<sup>th</sup> of March. The median values are indicated with horizontal red lines, the blue box resembles the lower and upper 25<sup>th</sup> and 75<sup>th</sup> percentiles, the whiskers represent the lowest and highest values considered for data evaluation, and the outliers are marked with red plus marks. The a.g. stands for above ground.

3.3 Analysis of measured and modelled concentrations

In the next sections, we present various results where modelled and measured pollutant concentrations are compared. The modelled and observed average pollutant concentrations for BC, PM<sub>10</sub>, LDSA, and PNC are shown in Fig. 8 for the 6 or 4 measurement poles, depending on the pollutant species, over the whole measurement campaign period. The split between emission source categories is shown for the model predictions in the form of staggered columns. With regards to the modelled emission source categories, “RWC” stands for residential wood combustion, and the category “Other” stands for a collection of minor source categories such as shipping, power plants and aviation. It should be noted that the averaging period varies between the measured pollutant species, and as such, the cross-comparison of e.g., BC and PM<sub>10</sub> at pole O10m should be avoided. The model predictions are affected by the measurement input in the whole Helsinki metropolitan area via the data assimilation procedure, while the campaign measurements have been excluded from the data assimilation. However, the campaign measurements for PM<sub>10</sub>, LDSA and PNC behind the noise barrier were utilised in a separate prior study to optimise the necessary hyperparameters for Eqs. 1-2. This means that the hourly emissions factors and regional scale background are constantly being adjusted based on the measurement evidence that is obtained outside of the campaign site. The model evaluation against the reference air quality stations that provide this input (up to 12 stations, depending on pollutant species) has been excluded from this paper and will be published separately.

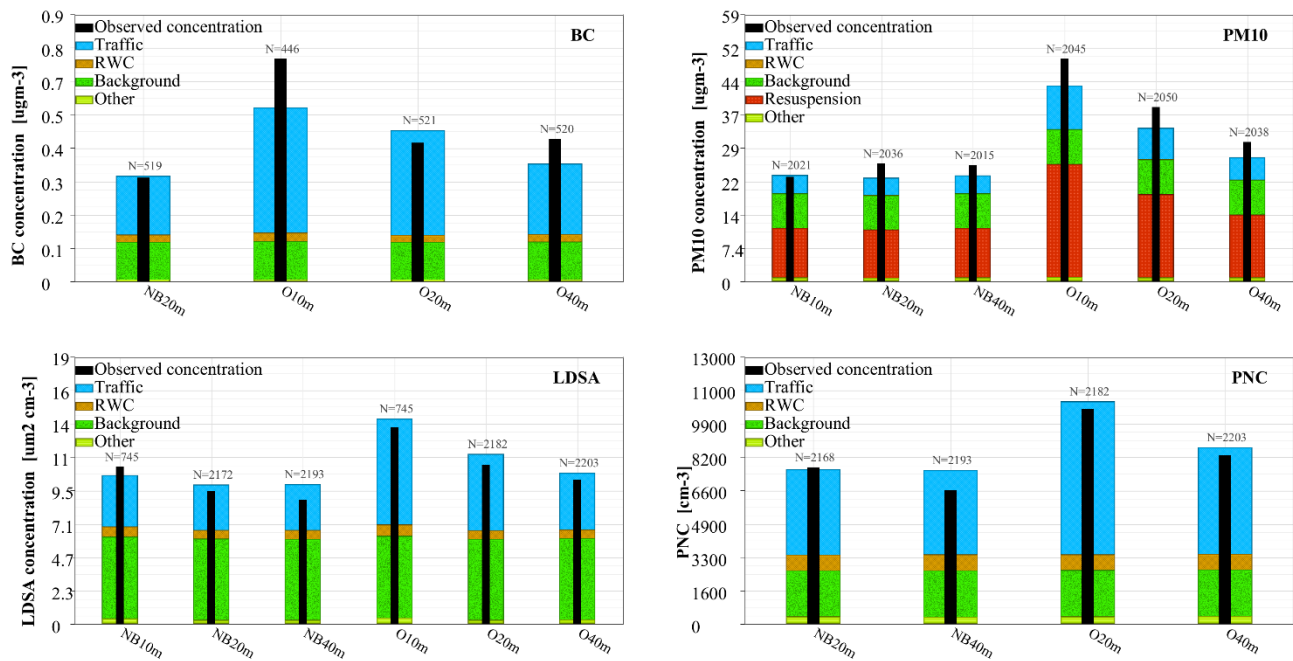


Figure 8: Modelled and observed average BC, PM<sub>10</sub>, LDSA and PNC during the campaign at the different measurement poles. The number of hourly data points forming the average for each pole and pollutant species has been shown as a number on top of the column.

The most notable difference between the modelled concentrations and the measurements is that the model underestimates PM<sub>10</sub> concentration in all but one of the 6 measurement locations (NB10m). At NB10m, the modelled concentration is almost one-to-one with measured concentrations. The largest deviation of the model with measured concentrations in the case of BC is observed at O10m, where the average BC concentration is underestimated. Also, the model seems to expect a constant decrease for BC in the open area with increasing distance from the highway, whereas the measured concentrations were slightly higher at O40m compared to O20m. For PM<sub>10</sub>, the modelled and measured concentrations seem to agree mostly well, with no notable gradients behind the noise barrier and similar gradients in the open area with each other. Only the observed concentrations, especially in the open area, were higher. In the case of LDSA and PNC, the trends and concentrations of measured and modelled concentrations were very similar. The traffic-related particles had quite noticeable contributions to all BC, LDSA, PNC and PM<sub>10</sub>. For example, at O20m the traffic-related fractions are 70%, 45%, 69% and 75%, respectively. Additionally, in the case of PM<sub>10</sub>, the effect of traffic is accompanied by resuspended particles that correspond to half of the PM<sub>10</sub> observed behind the noise barrier and more than half of the PM<sub>10</sub> in the open area. The contribution of resuspension was not visible in the case of BC, LDSA or PNC. In the case of BC and PNC, the contribution from traffic dominated the contribution from the background, but in the case of LDSA, the contribution from the background exceeded the contribution of traffic at all other poles but the O10m pole.

### 3.4 Measured and modelled daily mean concentrations

The measured and modelled pollutant concentrations for the main measured pollutants BC, PM<sub>10</sub>, LDSA, PNC, and NO<sub>2</sub> are compared in Fig. 9 in the form of daily averages. On the left-hand side, we show results for the pole behind the noise barrier that is closest to the highway and has available data for the pollutant. On the right-hand side, we show results for the pole nearest to the highway in the open area that had data available for the current pollutant. For brevity, the other remaining measurement locations are omitted as they resemble one of these two presented plots. We will use this style of representation and selection of plots in other figures as well. With regard to the presented results in this work, we focus on the less studied BC, PNC, LDSA and the more commonly studied PM<sub>10</sub>.

As can be seen from Fig. 9, the amount of BC data is relatively low and thus the results attained for BC should be considered slightly more uncertain compared to results related to the other measured variables. For BC, the daily mean concentrations varied between approximately 0.1 and 0.8  $\mu\text{g m}^{-3}$  behind the barrier and between 0.2 and 1.8  $\mu\text{g m}^{-3}$  in the open area. During the measurement period, frequent increases were seen in the PM<sub>10</sub> concentrations, especially during the dry periods in March and April. These episodes could be affected by resuspension of road pavement ground by studded tyres and salt that are used on the roads in wintertime to prevent slippery road conditions. This has been shown to result in frequent road dust episodes in springtime next to roads in Finland (Pirjola et al., 2010). The frequency of PM<sub>10</sub> episodes decreased in May, likely due to effective road cleaning in the area, and natural cleaning of the roads by rain and wind, with the reduction in the use of studded tyres. During the measurement period, daily averages for PM<sub>10</sub> reached 180  $\mu\text{g m}^{-3}$  in the open area. But starting from late April, these peaks were notably lower with PM<sub>10</sub> staying below 70  $\mu\text{g m}^{-3}$ . The high concentrations in early April may have

435 been enhanced due to the lack of rain. Behind the barrier, the concentrations were generally lower, with concentrations reaching over  $90 \mu\text{g m}^{-3}$  in early April but later staying mostly below  $40 \mu\text{g m}^{-3}$ . For LDSA, the observed concentrations behind the barrier and in the open area were at similar levels, being only slightly lower behind the noise barrier with a daily average reaching up to  $23 \mu\text{m}^{-2} \text{cm}^{-3}$ . For PNC, the concentrations were somewhat smaller behind the noise barrier, especially the observed daily maximum concentrations that reached  $21000 \text{ cm}^{-3}$  behind the noise barrier compared to  $30000 \text{ cm}^{-3}$  in the open

440 area.

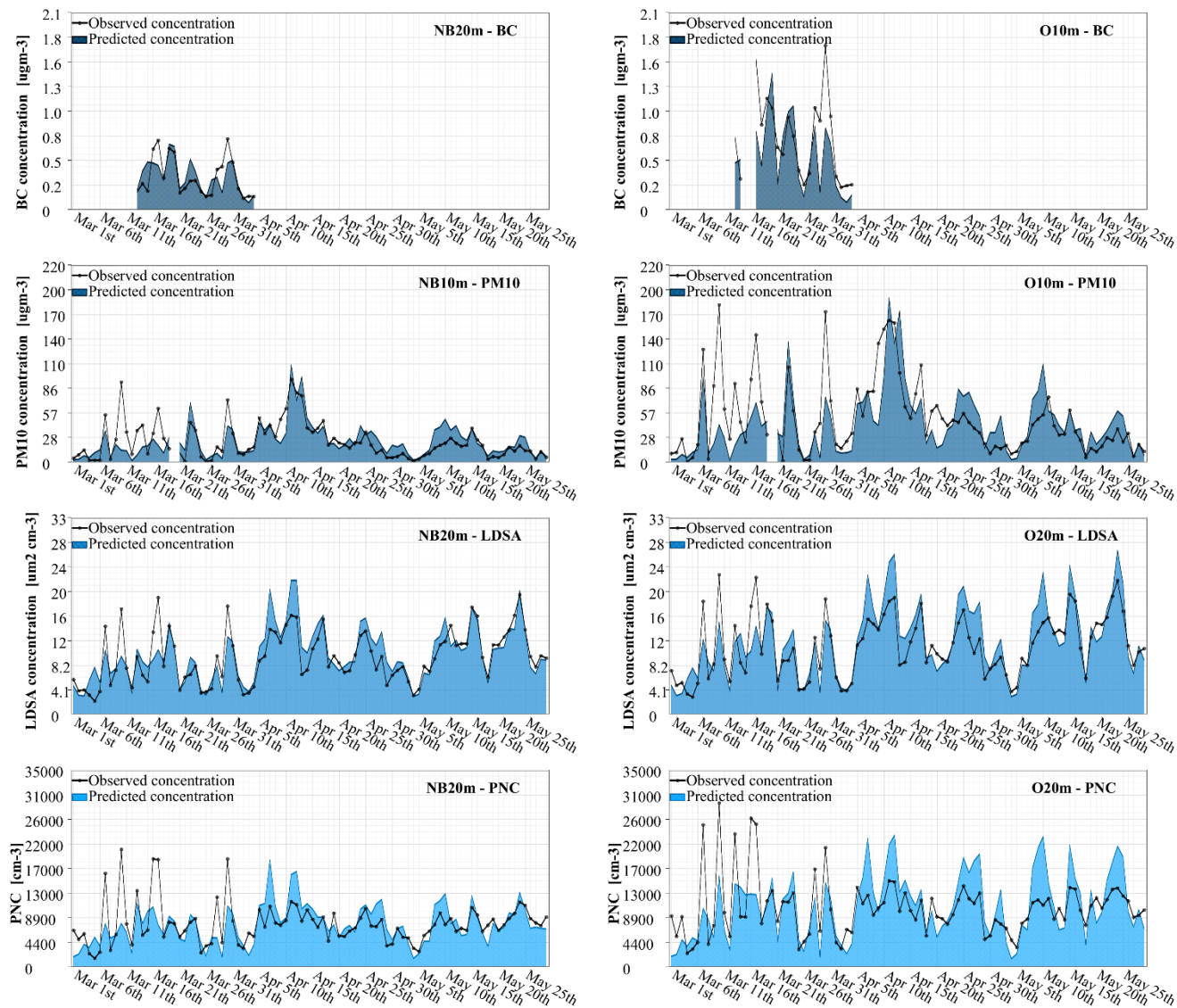


**Figure 9: Modelled and observed daily average pollutant concentrations of BC, PM10, LDSA and PNC for selected measurement locations (NB20m or NB10m and O20m or O10m).**

445 Fig. 9 shows that the model has the tendency to underpredict PM<sub>10</sub>, LDSA and PNC before the end of March. After April, however, the model has the tendency to overpredict concentrations, especially with PNC and LDSA. The underestimations of concentrations were most notable during days with the highest concentrations in March. This phenomenon was visible in all the pollutants, but most clearly in PM<sub>10</sub>. These further underline that there seem to be some difficulties in modelling the road PM<sub>10</sub> emissions during snow cover and the use of studded tyres. The simultaneous under-prediction of PNC during this time  
450 could also indicate difficulties in the modelling of atmospheric stability and local wind during winter conditions. During the low-concentration days, the agreement between the modelled and measured results was better. Interestingly, the weather also got drier approximately at the same time (Fig. 2). For BC, the change of model accuracy could not be evaluated as the data is limited to only March. However, during that time, the time series of the observed and predicted concentrations were very similar behind the noise barrier. However, in the open area, the model seems to underestimate the BC concentrations. When  
455 comparing the modelled and measured daily concentration averages, it is seen that the model agrees with the measured data better during April and May compared to March.

In Table 1, two chosen accuracy indicators (Factor-of-two, Pearson correlation) for the hourly modelled concentration against the sensor measurements (all locations) have been presented. There was a strong hourly variability in the measurement data that could not be captured by the model. None of the 6 measurement locations stands out, showing that the modelling accuracy  
460 was evenly matched in all locations. The most challenging hourly variability to model could be observed with O10m measuring PM<sub>10</sub>; approximately half of the time, the ratio of the measurement and the observed concentration was between 0.5 and 2. LDSA had clearly the highest agreement in terms of Pearson correlation as well as with the Factor-of-two indicator, while the worst correlation could be observed with PNC. Interestingly, the modelling of both LDSA and PNC relies on proxy information for emission factors and data assimilation-based learning, and this approach works well with LDSA but is less effective with  
465 PNC.

**Table 1: Accuracy indicators for hourly modelled and measured concentrations for PM<sub>10</sub>, LDSA, PNC and BC. FAC2 stands for Factor-of-two, and PCC stands for Pearson correlation coefficient. The definitions of these indicators can be found in the Supplements.**

	PM <sub>10</sub>		LDSA		PNC		BC	
	FAC2	PCC	FAC2	PCC	FAC2	PCC	FAC2	PCC
NB10m	0.60	0.53	0.88	0.56				
NB20m	0.61	0.55	0.89	0.62	0.73	0.40	0.68	0.53
NB40m	0.63	0.57	0.88	0.64	0.73	0.38		
O10m	0.51	0.55	0.87	0.67			0.61	0.55
O20m	0.56	0.60	0.86	0.63	0.71	0.50	0.65	0.55
O40m	0.62	0.62	0.88	0.64	0.73	0.43	0.64	0.49

470

### 3.5 Diurnal variability of pollutant concentrations

The average diurnal profiles for the selected pollutants are presented in Fig. 10. Similar plots for PM<sub>2.5</sub> and NO<sub>2</sub> are included in the supplementary material. Additionally, the supplementary material provides a breakdown of the modelled diurnal profiles by emission source categories. Diurnal profiles for the measured and modelled results are presented separately for BC, PM<sub>10</sub>,  
475 LDSA and PNC for all available poles. It is important to note that these pollutants do not have completely overlapping time series, which might contribute to slight differences in their diurnal patterns. This issue is particularly relevant for BC, which has data only for March. The modelled contributions from different sources to the diurnal profiles are presented in Supplement S1 and discussed in the related text.

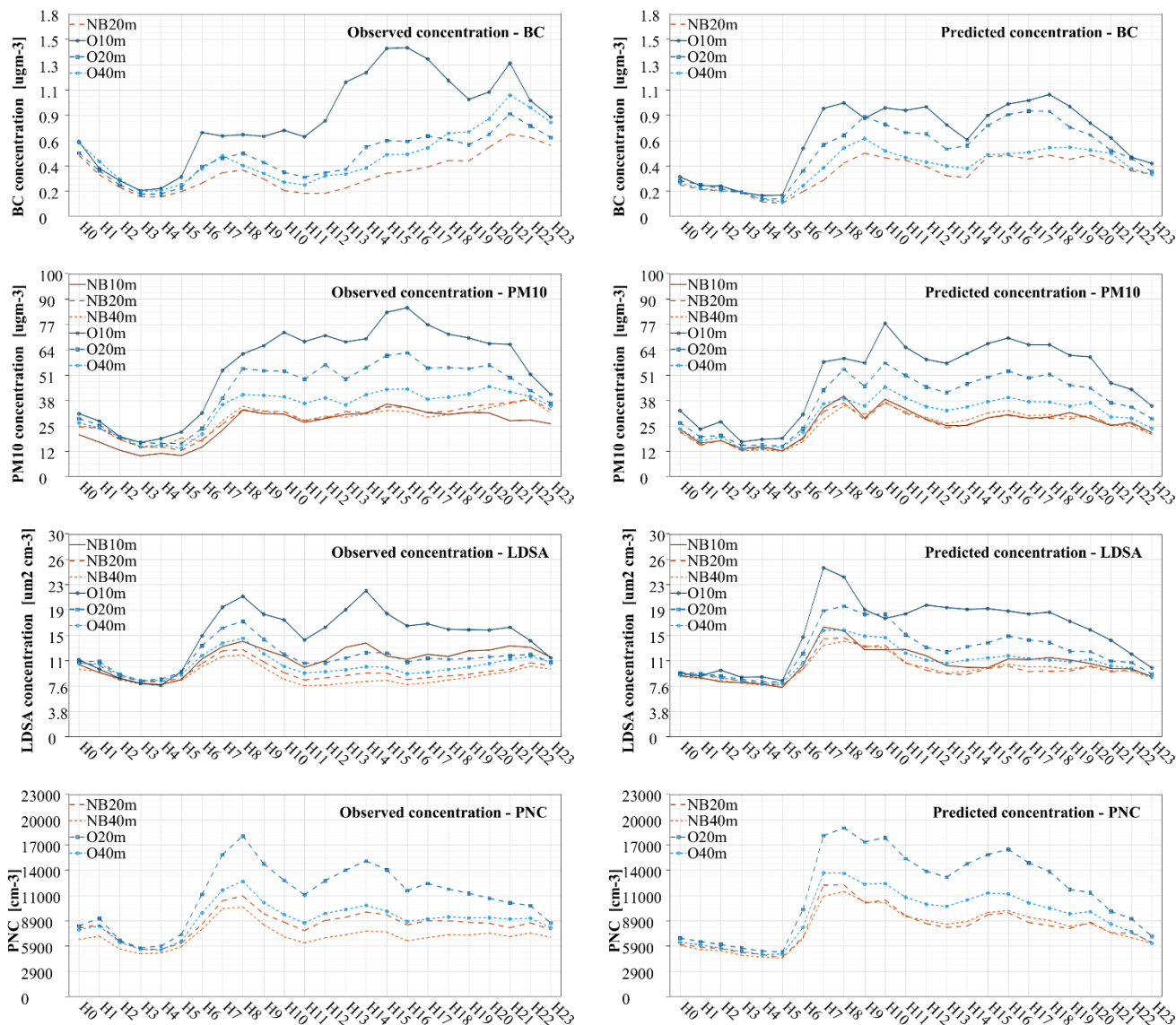


**Figure 10: Average diurnal variation of modelled and measured concentrations for BC, PM<sub>10</sub>, PNC and LDSA presented separately for all available measurement poles.**

When compared to the measured and modelled BC diurnal profiles, the modelled concentrations were consistently lower at all the poles and had similar diurnal patterns with traffic having minor peaks in the morning and evening rush hours at around 8 am and 4 pm. The observed BC concentrations peaked at approximately  $1.5 \mu\text{g m}^{-3}$  at 4 pm and reached a minimum of around  $0.2 \mu\text{g m}^{-3}$  at 3 am. In contrast, the modelled BC concentration had a maximum of  $1.0 \mu\text{g m}^{-3}$ , notably lower than the observed values. Additionally, the observed BC concentrations showed a second peak around 9 pm, with a concentration of  $1.3 \mu\text{g m}^{-3}$ , which was not observed in the modelled BC diurnal. Both modelled and measured BC concentrations showed a similar

minimum of  $0.2 \mu\text{g m}^{-3}$  during the early morning hours, with negligible differences between poles at this time. A noticeable  
490 difference between the modelled and measured concentrations lies in their gradients. In this sense, for the modelled  
concentrations, the decrease was gradual with increasing distance from the highway, and concentrations were lower behind  
the noise barrier. In contrast, for the observed concentrations, most of the reduction occurred between the O10m and O20m  
poles, with relatively similar concentrations at the other poles.

495 For  $\text{PM}_{10}$ , the modelled and measured diurnals had similar shapes, with concentrations reaching a minimum in the early  
morning hours and being elevated with the traffic. The measured  $\text{PM}_{10}$  reached its maximum of around  $85 \mu\text{g m}^{-3}$  during the  
afternoon rush hour and the minimum value below  $20 \mu\text{g m}^{-3}$  during the early morning hours. The modelled  $\text{PM}_{10}$   
concentrations reached their maximum of approximately  $75 \mu\text{g m}^{-3}$  at 10 am, and a minimum value below  $20 \mu\text{g m}^{-3}$  similarly  
to the measured  $\text{PM}_{10}$  in the early morning hours. The diurnal pattern of all the poles was very similar, with only the  
500 concentrations decreasing with increasing distance from the highway.

The observed LDSA concentration had a bimodal diurnal with two distinct modes at 8 am and 2 pm with concentrations of 21  
and  $22 \mu\text{m}^{-2} \text{cm}^{-3}$ , respectively. Whereas the modelled LDSA diurnal had only one clear mode at 7 pm with concentrations of  
 $25 \mu\text{m}^{-2} \text{cm}^{-3}$ . During the afternoon, the modelled LDSA was also elevated with concentrations around  $18\text{--}20 \mu\text{m}^{-2} \text{cm}^{-3}$ , but  
505 no clear mode was visible. Both the observed and modelled LDSA concentrations reached the minimum at around 4-5 am,  
with the concentrations around  $9 \mu\text{m}^{-2} \text{cm}^{-3}$  for both. Similar concentrations for traffic environments have also been reported  
in cities of Helsinki ( $13.2 - 35.4 \mu\text{m}^{-2} \text{cm}^{-3}$ ) and Tampere ( $12.2 - 47.9 \mu\text{m}^{-2} \text{cm}^{-3}$ ) (Kuula et al., 2020; Lepistö et al., 2023).  
Similar LDSA concentrations ( $9.4 \mu\text{m}^{-2} \text{cm}^{-3}$ ) to the minimum have been observed in urban background areas in Helsinki  
(Kuula et al., 2020). In Helsinki, in residential areas, the LDSA concentrations are measured between the urban background  
510 and traffic environments at  $12 - 22.6 \mu\text{m}^{-2} \text{cm}^{-3}$  (Kuula et al., 2020; Lepistö et al., 2023). Similar concentrations of  $22.5 \mu\text{m}^{-2}$   
 $\text{cm}^{-3}$  at residential areas have also been measured at Raahe (Lepistö et al., 2023). Modelled LDSA concentrations have earlier  
been compared to measured LDSA concentrations in Finland at traffic environment and urban background, with mean absolute  
errors of  $3.7$  and  $2.3 \mu\text{m}^{-2} \text{cm}^{-3}$ , respectively (Fung et al., 2022).

515 The peak for observed diurnal PNC was around  $19000 \text{ cm}^{-3}$ , and it was observed around 8 am. The second mode peak of the  
PNC was observed at around  $15000 \text{ cm}^{-3}$  at 2 pm. The modelled PNC showed similar diurnal and maximum values to the  
measured ones, with a maximum of around  $20000 \text{ cm}^{-3}$  at 7 am and an afternoon peak of  $17000 \text{ cm}^{-3}$  at 4 pm. Both the modelled  
and observed diurnals had their minimum in the early morning hours and PNC of around  $5000 \text{ cm}^{-3}$ . Notably, in the case of  
observations, NB40 had a lower concentration than NB20 during the whole day, whereas in the case of modelled PNC, NB40  
520 and NB20 had very similar concentrations throughout the day. In the case of observed concentrations, there was a reduction  
in PNC when moving further away from the highway and the lowest PNC were measured behind the noise barrier.



Overall, the modelled and measured diurnal profiles were quite similar, and the largest differences were observed for the BC concentrations. For all the pollutants, the lowest concentrations were measured during the early morning hours before the traffic started to increase, and the highest concentrations were during the daytime, indicating strong contributions from traffic. All the measured pollutants BC, PM<sub>10</sub>, LDSA and PNC also reached similar concentrations at each of the poles during the early morning hours. This enhances the trustworthiness of the sensor results, as during this period, when traffic's contribution to concentrations was minimal, the sensors were effectively performing collocated measurements. Under these conditions, the sensors should display similar concentration readings if the instruments are functioning properly. Additionally, the model results during this time were on a very similar level to the measured results, which implies that both the model and sensors were effective in measuring the background concentrations.

### 3.6 Modelled and measured concentrations as a function of wind direction

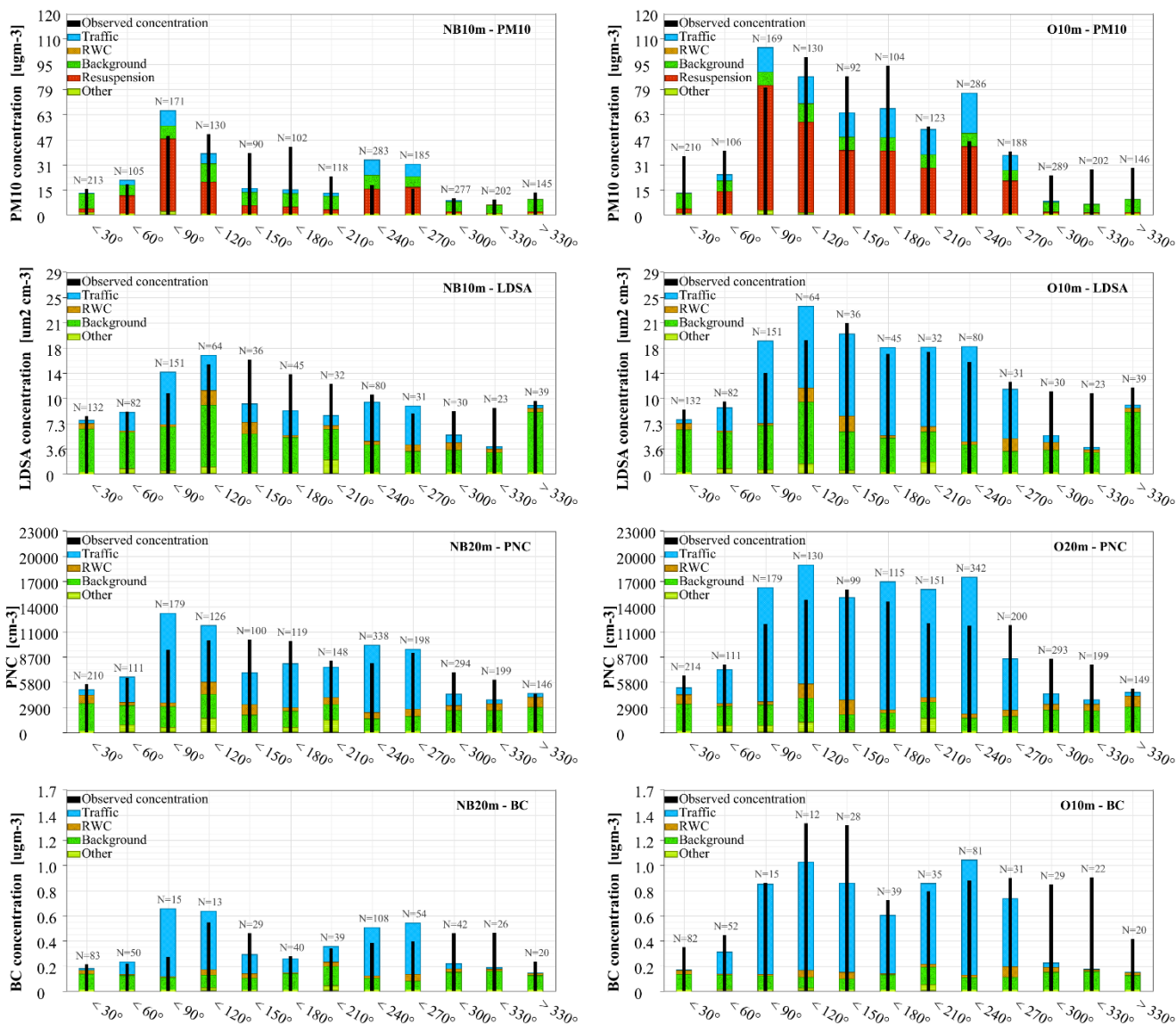
In Fig. 11, conditional averages as a function of wind direction for measured and modelled concentration are shown for PM<sub>10</sub>, LDSA, PNC and BC. Again, on the left-hand side, we show the concentrations behind the noise barrier and at the open area on the right-hand side. HARMONIE NWP meteorology was used in the modelling, and thus the presented averages are based on HARMONIE wind directions. There are an unequal number of data points for different wind directions; at worst, for BC measurements, there are only 20 data points available to compare measured and modelled hourly concentrations when the wind direction is between 330 to 360°. The measurement site was located on the northern side of the highway that was oriented in the West-southwest to East-northeast direction, and therefore, when the wind is blowing between approximately directions of 90 to 225°, the air mass passes over the highway.

As expected, the traffic emissions (and resuspension of particles) were most prevalent with wind directions between 90 to 270° that corresponded to the location of the highway from the measurement site. As can be seen from the results for NB10m, the model overestimated the blocking effect of the barrier (i.e., the model underestimated concentration) when the wind direction was orthogonal to the highway. Similarly, when the wind was blowing directly from the highway, the PM<sub>10</sub> concentrations were underestimated at O10m. When the wind was not blowing from the direction of the highway, the model under-predicted PM<sub>10</sub> at the O10m pole. This could indicate that the model underestimated the effect of speed on PM<sub>10</sub> emissions from the highway, as the high-speed limit at the site is 100 km/h, which is unique in the Helsinki metropolitan area measurement locations and no similar underestimations are observed at reference stations.

The model also underpredicted the PM<sub>10</sub> concentrations between 300 and 30 degrees in the open area. Similar underprediction was not observed behind the noise barrier. The under-prediction of concentrations in the wind directions 300 to 360 was not limited to PM<sub>10</sub> but was also observed for LDSA, PNC and BC. For LDSA, PNC and BC, underestimation of concentrations was also observed behind the noise barrier. The most notable underestimation was observed for BC at O10m with wind directions between 300 to 360 degrees (which was the direction of the storage building behind the measurement area), possibly indicating that there was a combustion source in this direction that was not considered by the model. In the case of BC, the

source could have been car workshops on the roadside of the storage building situated behind the measurement site in this direction. The cars running in front of these workshops could have caused some elevated concentration when the wind was blowing from this direction.

560 Underestimation of concentrations at O10 might also indicate contributions from traffic to even when the wind was not coming from the direction of the highway, which the model was not able to capture. Also, any dry surface with resuspension particles can act as a dust source given sufficient meteorological conditions, but this possibility has been omitted from the model. Despite the observed differences, the simplistic treatment of the noise barrier in a Gaussian dispersion model still results in a reasonable agreement between measured and modelled concentrations.



565 **Figure 11: Modelled contributions of different sources to PM<sub>10</sub>, LDSA and PNC and observed concentrations at different poles as a**  
**function of ambient wind direction (HARMONIE NWP). The first wind direction (< 30°) contains data points when the wind has**  
**blown from a direction that is between North (0°) and 30 degrees from North towards East.**

### 3.7 NO<sub>2</sub> Passive samplers

To capture the effect of exhaust gases around the measurement area. The NO<sub>2</sub> concentrations were measured via the passive  
 570 samplers (locations shown in Fig. 1). In Fig. 12, the measured and modelled NO<sub>2</sub> concentrations are presented for data averaged  
 over February, April and May. The results during March suffered from quality issues and have therefore been omitted from  
 this paper. The highest observed and modelled concentrations are seen for PAS\_6m, which was located on the roadside of the

noise barrier in the proximity of the highway. This location is especially challenging for Gaussian models, as the close by noise barrier can affect the micrometeorology near the road. Overall, the modelled and measured NO<sub>2</sub> concentrations were in good agreement, especially in the locations behind the noise barrier. The largest differences were observed for the poles closest to the highway (PAS\_010m, PAS\_O20m and PAS\_6m). The measured NO<sub>2</sub> averages were consistently lower than the measured concentrations. Further, in open areas, the decreasing trend of NO<sub>2</sub> is quite minor while the model suggests a more intuitive and expected decreasing trend as a function of distance. Additionally, the NO<sub>2</sub> concentrations measured at the poles with passive samplers were lower compared to the measurements used for calculating the gradients. The lowest concentrations both modelled and measured were seen for PAS\_100m, which was the pole situated furthest from the road.

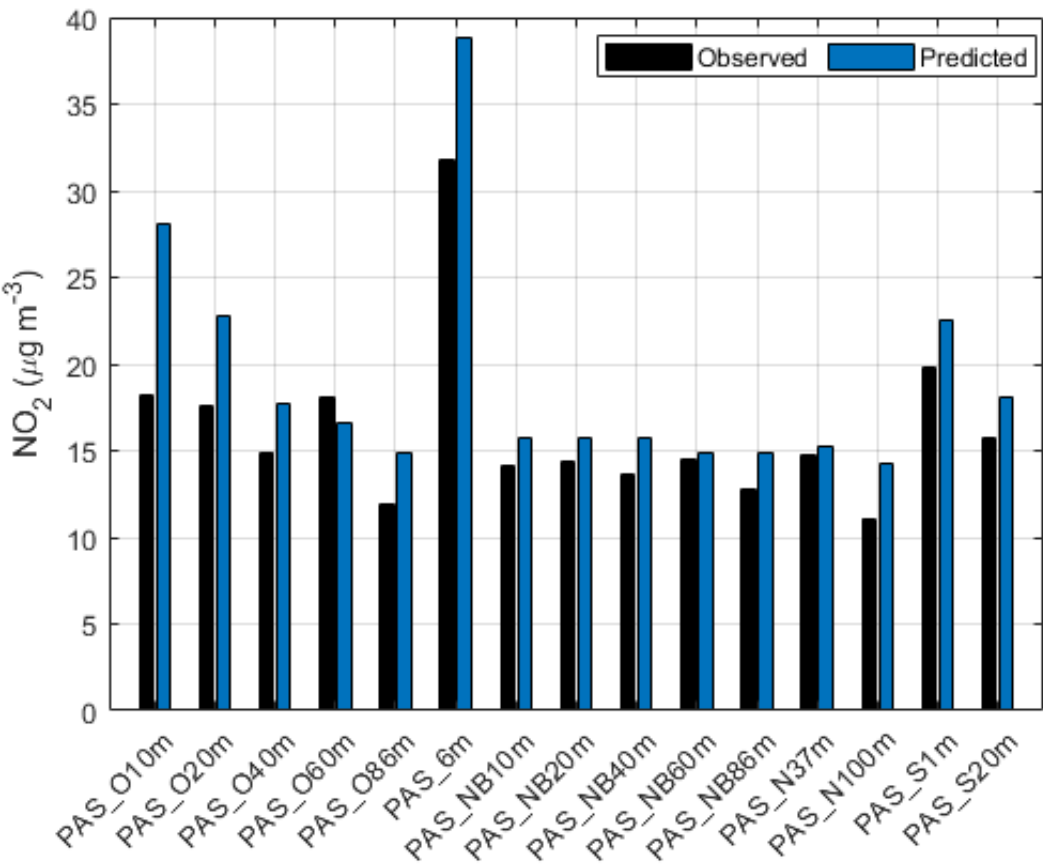


Figure 12: Observed concentrations (µm m<sup>-3</sup>) with passive NO<sub>2</sub> samplers compared against Enfuser predictions for data averaged over February, April and May.

### 3.8 Modelled geographical distribution of pollutants

In Fig. 13, the modelled concentrations (at 2 m above ground) are presented around the Helsinki metropolitan area and in more detail around the measurement site. We have selected to show the PM<sub>10</sub> monthly average concentrations for April. However,

similar geographical distributions are available for all focused pollutant species and for all months during the campaign period. The presented monthly average has been processed from hourly concentration distributions as the Enfuser model estimates these as its main, publicly available output.

590

The model predicted the highest concentrations overall in the Helsinki area around the largest highways, with the concentration scale reaching up to  $100 \mu\text{g m}^{-3}$ . Overall, the concentrations were seen to decrease quite sharply with increasing distance from highways on a large scale. In the zoomed-in figure of the measurement location, the noise barriers are seen in the figure as light green lines (very low concentrations at the location of the barrier) on the northern side of the highway. In the figure, the effects of utilising Eqs. 1-3 can be seen in the area where the gap in the noise barrier is located; the modelled concentrations in the gap are clearly higher than the ones behind the barrier. Further, the modelled concentration behind some of the buildings is also reduced due to the obstacle reduction method, showing that the capability is not limited to specific obstacles such as noise barriers.

595

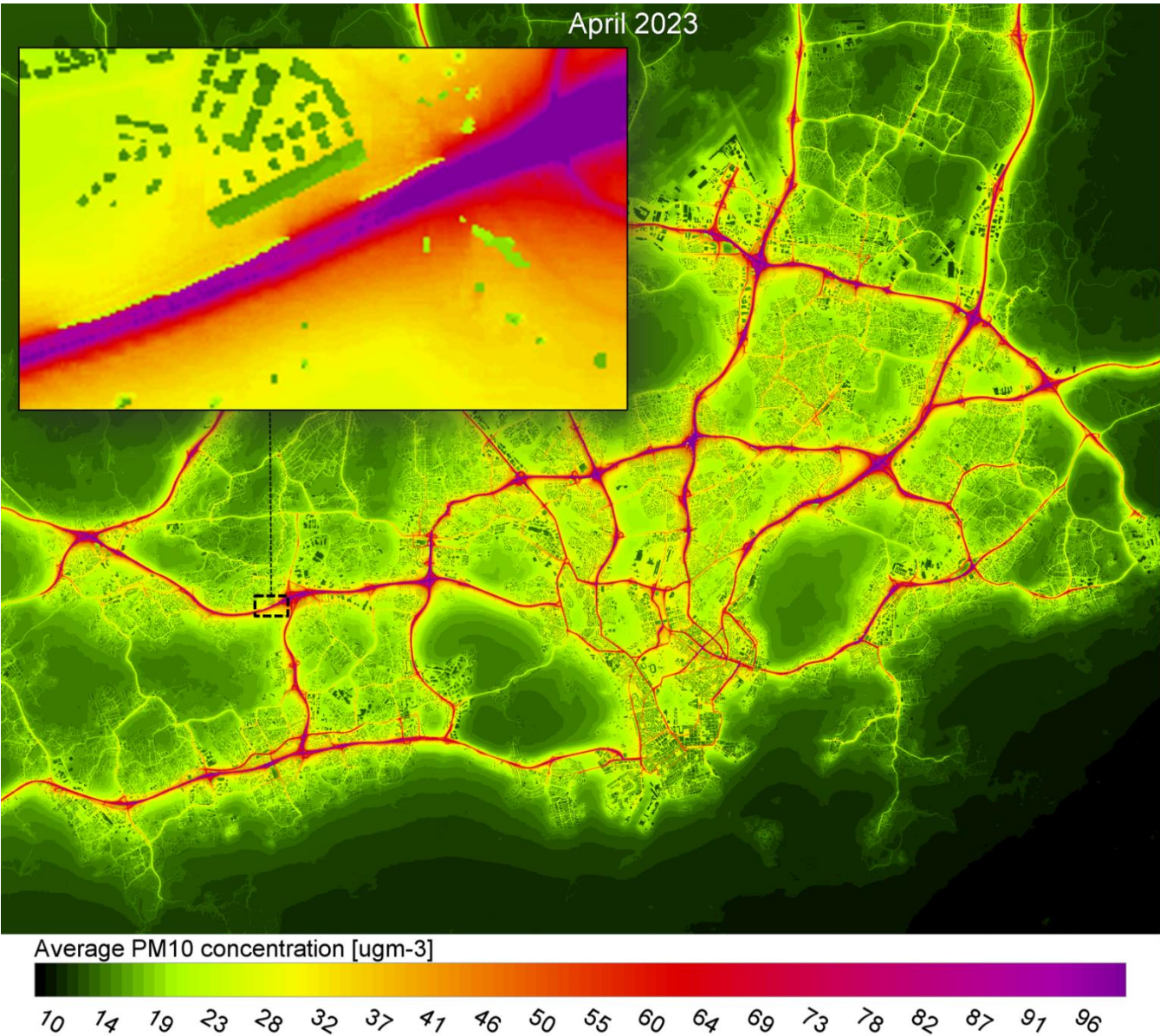


Figure 13: Modelled average PM<sub>10</sub> concentrations during April 2023 in the overall Helsinki metropolitan area and near the measurement campaign site.

4. Conclusions

Overall, the noise barrier of 6.5 m in height was found to be effective in reducing the measured concentration of pollutants behind the barrier. The concentrations behind the noise barrier were lower for all the measured pollutants, PM<sub>10</sub>, PM<sub>2.5</sub>, PNC, LDSA, BC and NO<sub>2</sub>. The difference between the open area and the area behind the noise barrier was the largest for PM<sub>10</sub> and

the smallest for NO<sub>2</sub>. Measurement data also showed that concentrations of all pollutants decreased as a function of distance from the highway, with the steepest gradients being observed nearest to the highway. The decreasing gradient was strongest for the PM<sub>10</sub> and least noteworthy for NO<sub>2</sub> behind the noise barrier. The decreasing gradients were less clear, and for example, PM<sub>10</sub> had the lowest concentrations closest to the road at NB10 pole, with higher concentrations at NB20 and NB40. Indicating that the noise barrier effectively blocks the dispersion of PM<sub>10</sub> from the road, but when the distance to the road increases, the concentrations from the open area get mixed with the airmass again elevating the concentrations.

Modelled concentrations of all pollutants showed good agreement with measurements. This success can partly be attributed to tailored modelling of nearby traffic flows, which were adjusted to match the real vehicular flow data. This flow customisation was performed separately for the two traffic flow directions and for passenger cars and heavy vehicles. The largest difference between modelled and measured pollutants was observed for PM<sub>10</sub>, which was underestimated compared to the measurement near the campaign site. This may indicate that the model underestimates the speed dependency of coarse particle emissions, as the high-speed limit of 100 km/h at this site is unique in the Helsinki metropolitan area and no similar underestimation was observed at other reference stations (not shown in this paper). Another notable underestimation by the model was observed with BC in the pole closest to the highway in the open area.

The noise barrier was considered in the modelling by defining it as an obstacle. A statistical reduction for concentrations was applied based on the distance from the emitter to the obstacle and the height difference between the obstacle and the emitter. The simplified modelling approach captured the real-life effect of the noise barrier; however, more research would be needed to generalise and properly parametrise the approach. The simplistic reduction model used two hyperparameters that were calibrated based on the measurement data, using Monte Carlo simulation. In this simulation, the parameter values were varied to find an optimal state that results in as low as possible prediction error in terms of RMSE for PNC, PM<sub>10</sub> and LDSA. Only a handful of values for each hyperparameter were tested, as the overfitting of a simple statistical reduction model with only a few measurement locations providing calibration data should be avoided. Another limitation of the optimal parameter assessment comes from the fact that the barrier height was constant, i.e., the applicability of the simple model remains untested with different barrier heights. Nevertheless, the simplistic reduction model has room for improvement, provided that a more thorough training set is available. One option is to utilise the CFD models' output and calibrate a more generalised reduction method if steady-state concentrations provided by the CFD model (e.g., a LES model) are realistic proxies for true concentrations.

The modelled NO<sub>2</sub> average was compared against passive NO<sub>2</sub> measurements. According to the results, these were in general agreement with the exceptions in two samplers close to the highway (PAS\_6m and PAS\_O10m). With these two samplers, a strong overprediction was seen during February and April, but not during May. These discrepancies may have been the result of simplified in-plume NO<sub>x</sub>-Ozone photochemistry that is being used in Enfuser and meteorological effects affecting the

passive samplers. It is also possible that the passive sampler measurements during April were biased indicators for true concentrations. In this paper, we have demonstrated the benefits of combining measurements and modelling approaches in the analysis of air quality. The measurement data can be used to improve modelling capabilities, and the modelling results help to understand and analyse the obtained measurement data.

## 645 **Author contributions**

SH, LJ, JVN, TP, and HT contributed to conceptualisation. SH, LJ, JVN, VS, VL and JACV handled data curation. SH and LJ performed the formal analysis of the data. TP and HT were responsible for the funding acquisition. SH, JVN, VS, JACV, KL, VL, KD and DB handled the investigation. LJ contributed to the methodology, model development and used the model for output creation. TR, HEM, TP and HT were responsible for project administration. SH and LJ handled the visualisation  
650 and writing the original draft. All of the authors also contributed to review and editing review and editing.

## **Acknowledgements**

We thank Jussi Hoivala and Jyrki Widenius for their help in experiments. This work was supported by Technology Industries of Finland Centennial Foundation (Urban Air Quality 2.0 project), European Union Horizon 2020 research and innovation programme under grant agreement No 101036245 (RI-URBANS), European Union's Horizon Europe research and innovation  
655 programme grant agreement No 101096133 (PAREMPI), Academy of Finland via the project Black and Brown Carbon in the Atmosphere and the Cryosphere (BBrCAC) (decision nr. 341271) and Flagship Funding (grant no. 337552, 337551, 337549).

## **Code availability**

Source code of the Enfuser model is publicly available via GitHub under the MIT license: <https://github.com/johanssl/EnfuserMIT.git>. The repository contains the necessary code and input data for operative modelling of  
660 air quality in the Helsinki metropolitan area.

## **Data availability**

Data produced for the Helsinki Metropolitan Area by the model is publicly available via the Open Data portal of FMI (FMI, 2024).



### 665 Competing interests

At least one of the (co-)authors is a member of the editorial board of Atmospheric Chemistry and Physics.

### References

- Ayers, G.P., Keywood M.D., Gillett, R., Manins, H., Malfroy, H., and Bardsley, T.: Validation of passive  
670 diffusion samplers for SO<sub>2</sub> and NO<sub>2</sub>, *Atmos. Environ.*, 32, 3587–3592, [https://doi.org/10.1016/S1352-2310\(98\)00079-X](https://doi.org/10.1016/S1352-2310(98)00079-X) 1998.
- Baensch-Baltruschat, B., Kocher, B., Stock, F., & Reifferscheid, G.: Tyre and road wear particles (TRWP) - A review of  
generation, properties, emissions, human health risk, ecotoxicity, and fate in the environment, *Sci. Total Environ.* 733, 137823,  
<https://doi.org/10.1016/j.scitotenv.2020.137823>, 2020.
- Baldauf, R. W., Isakov, V., Deshmukh, P., Venkatram, A., Yang, B., & Zhang, K. M.: Influence of solid noise barriers on  
675 near-road and on-road air quality, *Atmos. Environ.*, 129, 265–276, <https://doi.org/10.1016/j.atmosenv.2016.01.025>, 2016.
- Bengtsson, L., Andrae, U., Aspelien, T., Batrak, Y., Calvo, J., Rooy, W. de, Gleeson, E., Hansen-Sass, B., Homleid, M., Hortal,  
M., Ivarsson, K. I., Lenderink, G., Niemelä, S., Nielsen, K. P., Onvlee, J., Rontu, L., Samuelsson, P., Muñoz, D. S., Subias,  
A., Tijm, S., Toll, V., Yang, X., and Koltzow, M. Ø. The HARMONIE-AROME model configuration in the ALADIN-  
HIRLAM NWP system, *Mon. Weather. Rev.*, 145(5), 1919–1935, <https://doi.org/10.1175/MWR-D-16-0417.1>, 2017.
- 680 Brechtel Manufacturing Inc. BMI Model 1720 MCPC Manual (Version 2.2), [https://www.brechtel.com/wp625content/uploads/2021/08/bmi\\_model\\_1720\\_mcpc\\_manual\\_v2.2.pdf](https://www.brechtel.com/wp625content/uploads/2021/08/bmi_model_1720_mcpc_manual_v2.2.pdf) (2021).
- Brus, D., Gustafsson, J., Vakkari, V., Kemppinen, O., de Boer, G., and Hirsikko, A.: Measurement report: Properties of aerosol  
and gases in the vertical profile during the LAPSE-RATE campaign, *Atmos. Chem. Phys.*, 21, 517–533,  
<https://doi.org/10.5194/acp-21-517-2021>, 2021.
- 685 Caubel, J. J., Cados, T. E., Preble, C. V., and Kirchstetter, T. W.: A Distributed Network of 100 Black Carbon Sensors for 100  
Days of Air Quality Monitoring in West Oakland, California, *Environ. Sci. Technol.*, 53, 7564–7573, 2019.
- Cheng, Y.H., and Lin, M.H.: Real-Time Performance of the microAeth® AE51 and the Effects of Aerosol Loading on Its  
Measurement Results at a Traffic Site, *Aerosol Air Qual. Res.* 13, 1853–1863, <https://doi.org/10.4209/aaqr.2012.12.0371>,  
2013.
- 690 Denby, B.R., Gauss, M., Wind, P., Mu, Q., Grøtting Wærsted, E., Fagerli, H., Valdebenito, A. and Klein, H.: Description of  
the uEMEP\_v5 downscaling approach for the EMEP MSC-W chemistry transport model, *Geosci. Model Dev.*, 13(12),  
<https://doi.org/10.5194/gmd-13-6303-2020>, 2020.

Denby, B. R., Ketzel, M., Ellermann, T., Stojiljkovic, A., Kupiainen, K., Niemi, J. V., Norman, M., Johansson, C., Gustafsson, M., Blomqvist, G., Janhäll, S., and Sundvor, I.: Road salt emissions: A comparison of measurements and modelling using the NORTRIP road dust emission model, *Atmos. Environ.*, 141, 508–522, <https://doi.org/10.1016/j.atmosenv.2016.07.027>, 2016.

DigiTraffic. Traffic measurement data available from: <https://www.digitraffic.fi/en/road-traffic/lam/>, data for road weather stations, available from <https://www.digitraffic.fi/en/road-traffic/#current-data-of-road-weather-stations>. (Visited 3<sup>rd</sup> of December 2024).

Directive - EU - 2024/2881, On ambient air quality and cleaner air for Europe, URL: <https://eur-lex.europa.eu/eli/dir/2024/2881/oj>, 2024.

Elomaa, T., Luoma, K., Harni, S., Virkkula, A., Timonen, H., and Petäjä, T.: Applicability of small-scale black carbon sensors to explore high resolution spatial variability of ambient black carbon, *Aerosol Research Discuss.* [preprint], <https://doi.org/10.5194/ar-2024-12>, in review, 2024.

Enroth, J., Saarikoski, S., Niemi, J., Kousa, A., Ježek, I., Močnik, G., Carbone, S., Kuuluvainen, H., Rönkkö, T., Hillamo, R., and Pirjola, L.: Chemical and physical characterization of traffic particles in four different highway environments in the Helsinki metropolitan area. *Atmos. Chem. Phys.*, 16(9), 5497–5512, <https://doi.org/10.5194/acp-16-5497-2016>, 2016.

European Air quality directive, <https://eur-lex.europa.eu/eli/dir/2024/2881/oj/eng>, (Accessed 10th June 2024).

Ferm M.: A sensitive diffusional sampler. IVL rapport L91-172, Göteborg, 1991.

FMI. The catalog for the Finnish meteorological institute’s open data portal. Visited. <https://en.ilmatieteenlaitos.fi/open-data-sets-available>. (Accessed 11th December 2024).

Fung, P. L., Zaidan, M. A., Niemi, J. V., Saukko, E., Timonen, H., Kousa, A., Kuula, J., Rönkkö, T., Karppinen, A., Tarkoma, S., Kulmala, M., Petäjä, T., and Hussein, T.: Input-adaptive linear mixed-effects model for estimating alveolar lung-deposited surface area (LDSA) using multipollutant datasets. *Atmos. Chem. Phys.*, 22(3), 1861–1882. <https://doi.org/10.5194/acp-22-1861-2022>, 2022.

Fussell, J. C., Franklin, M., Green, D. C., Gustafsson, M., Harrison, R. M., Hicks, W., Kelly, F. J., Kishta, F., Miller, M. R., Mudway, I. S., Oroumijeh, F., Selley, L., Wang, M., and Zhu, Y.: A Review of Road Traffic-Derived Non-Exhaust Particles: Emissions, Physicochemical Characteristics, Health Risks, and Mitigation Measures, *Environ. Sci. and Technol.*, 56(11), 6813–6835, <https://doi.org/10.1021/acs.est.2c01072>, 2022.

Gani, S., Bhandari, S., Patel, K., Seraj, S., Soni, P., Arub, Z., Habib, G., Hildebrandt Ruiz, L., and Apte, J. S.: Particle number concentrations and size distribution in a polluted megacity: the Delhi Aerosol Supersite study, *Atmos. Chem. Phys.*, 20, 8533–8549, <https://doi.org/10.5194/acp-20-8533-2020>, 2020.

Gren, L., Malmberg, V. B., Falk, J., Markula, L., Novakovic, M., Shamun, S., Eriksson, A. C., Kristensen, T. B., Svenningsson, B., Tunér, M., Karjalainen, P., and Pagels, J, Effects of renewable fuel and exhaust aftertreatment on primary and secondary emissions from a modern heavy-duty diesel engine, *J. of Aerosol Sci.*, 156, <https://doi.org/10.1016/j.jaerosci.2021.105781>, 2021.

- 725 Hellsten, A., Ketelsen, K., Sührling, M., Auvinen, M., Maronga, B., Knigge, C., Barmpas, F., Tsegas, G., Moussiopoulos, N., and Raasch, S.: A nested multi-scale system implemented in the large-eddy simulation model PALM model system 6.0. *Geoscientific Model Development*, 14(6), 3185–3214, <https://doi.org/10.5194/gmd-14-3185-2021>, 2021.
- Hilker, N., Wang, J. M., Jeong, C. H., Healy, R. M., Sofowote, U., Debosz, J., Su, Y., Noble, M., Munoz, A., Doerksen, G., White, L., Audette, C., Herod, D., Brook, J. R., and Evans, G. J.: Traffic-related air pollution near roadways: Discerning local  
730 impacts from background, *Atmos. Meas. Tech*, 12(10), 5247–5261, <https://doi.org/10.5194/amt-12-5247-2019>, 2019.
- HSY, air quality map, <https://www.hsy.fi/en/air-quality-and-climate/air-quality-now/air-quality-map/>, (Visited 3<sup>rd</sup> of December 2024).
- Johansson, L., Karppinen, A., Kurppa, M., Kousa, A., Niemi, J. V., and Kukkonen, J.: An operational urban air quality model ENFUSER, based on dispersion modelling and data assimilation, *Environ. Modelling and Softw*, 156,  
735 <https://doi.org/10.1016/j.envsoft.2022.105460>, 2022.
- Kangasniemi, O., Kuuluvainen, H., Heikkilä, J., Pirjola, L., Niemi, J. V., Timonen, H., Saarikoski, S., Rönkkö, T., and Maso, M. D.: Dispersion of a traffic related nanocluster aerosol near a major road, *Atmosphere*, 10(6), <https://doi.org/10.3390/atmos10060309>, 2019.
- Kassandros, T., Bagkis, E., Johansson, L., Kontos, Y., Katsifarakis, K.L., Karppinen, A., and Karatzas, K.: Machine learning-  
740 assisted dispersion modelling based on genetic algorithm-driven ensembles: An application for road dust in Helsinki, *Atmos. Environ.*, 307, 119818, <https://doi.org/10.1016/j.atmosenv.2023.119818>, 2023.
- Kupiainen, K., Ritola, R., Stojiljkovic, A., Pirjola, L., Malinen, A., and Niemi, J.: Contribution of mineral dust sources to street side ambient and suspension PM10 samples. *Atmos. Environ.*, 147, 178–189, <https://doi.org/10.1016/j.atmosenv.2016.09.059>, 2016.
- 745 Kumar, P., Fennell, P., and Britter, R.: Effect of wind direction and speed on the dispersion of nucleation and accumulation mode particles in an urban street canyon, *Sci. Total Environ.*, 402(1), 82–94. <https://doi.org/10.1016/j.scitotenv.2008.04.032>, 2008.
- Kuula, J., Kuuluvainen, H., Niemi, J. V., Saukko, E., Portin, H., Kousa, A., Aurela, M., Rönkkö, T., and Timonen, H.: Long-term sensor measurements of lung deposited surface area of particulate matter emitted from local vehicular and residential  
750 wood combustion sources, *Aerosol Sci. Technol.*, 54(2), 190–202, <https://doi.org/10.1080/02786826.2019.1668909>, 2020.
- Lepistö, T., Barreira, L. M. F., Helin, A., Niemi, J. V., Kuittinen, N., Lintusaari, H., Silvonen, V., Markkula, L., Manninen, H. E., Timonen, H., Jalava, P., Saarikoski, S., and Rönkkö, T.: Snapshots of wintertime urban aerosol characteristics: Local sources emphasized in ultrafine particle number and lung deposited surface area, *Environ. Res.*, 231, <https://doi.org/10.1016/j.envres.2023.116068>, 2023.
- 755 Lepistö, T., Lintusaari, H., Oudin, A., Barreira, L. M. F., Niemi, J. V., Karjalainen, P., Salo, L., Silvonen, V., Markkula, L., Hoivala, J., Marjanen, P., Martikainen, S., Aurela, M., Reyes, F. R., Oyola, P., Kuuluvainen, H., Manninen, H. E., Schins, R. P. F., Vojtisek-Lom, M., Ondracek, J., Topinka, J., Timonen, H., Jalava, P., Saarikoski, S., and Rönkkö, T.: Particle lung

- deposited surface area (LDSAal) size distributions in different urban environments and geographical regions: Towards understanding of the PM<sub>2.5</sub> dose–response. *Environ. Int.*, 180, <https://doi.org/10.1016/j.envint.2023.108224>, 2023.
- 760 Li, B., Qiu, Z., and Zheng, J.: Impacts of noise barriers on near-viaduct air quality in a city: A case study in Xi'an, *Build. Environ.*, 196, <https://doi.org/10.1016/j.buildenv.2021.107751>, 2021.
- Noll, K. E., Jackson, M. M., and Oskouie, A. K.: Development of an atmospheric particle dry deposition model, *Aerosol Sci. and Technol.*, 35(2), 627–636. <https://doi.org/10.1080/02786820119835>, 2001.
- OSM, OpenStreetMap raw data extraction, <https://www.openstreetmap.org/export>, (Visited 3<sup>rd</sup> of December 2024).
- 765 Petäjä, T., Ovaska, A., Fung, P. L., Poutanen, P., Yli-Ojanperä, J., Suikkola, J., Laakso, M., Mäkelä, T., Niemi, J. V., Keskinen, J., Järvinen, A., Kuula, J., Kurppa, M., Hussein, T., Tarkoma, S., Kulmala, M., Karppinen, A., Manninen, H. E., and Timonen, H.: Added Value of Vaisala AQT530 Sensors as a Part of a Sensor Network for Comprehensive Air Quality Monitoring, *Front. Environ. Sci.*, 9, <https://doi.org/10.3389/fenvs.2021.719567>, 2021.
- Pirjola, L., Johansson, C., Kupiainen, K., Stojiljkovic, A., Karlsson, H., and Hussein, T.: Road dust emissions from paved  
770 roads measured using different mobile systems, *J. Air Waste. Manag. Assoc.*, 60(12), 1422–1433, <https://doi.org/10.3155/1047-3289.60.12.1422>, 2010.
- Rolstad Denby, B., Gauss, M., Wind, P., Mu, Q., Grøtting Wærsted, E., Fagerli, H., Valdebenito, A., and Klein, H.: Description of the uEMEP\_v5 downscaling approach for the EMEP MSC-W chemistry transport model, *Geosci. Model Dev.*, 13(12), 6303–6323 <https://doi.org/10.5194/gmd-13-6303-2020>, 2020.
- 775 Rönkkö, T., Kuuluvainen, H., Karjalainen, P., Keskinen, J., Hillamo, R., Niemi, J. V., Pirjola, L., Timonen, H. J., Saarikoski, S., Saukko, E., Järvinen, A., Silvennoinen, H., Rostedt, A., Olin, M., Yli-Ojanperä, J., Nousiainen, P., Kousa, A., and Dal Maso, M.: Traffic is a major source of atmospheric nanocluster aerosol, *Proc. Natl. Acad. Sci. U.S.A.*, 114(29), 7549–7554, <https://doi.org/10.1073/pnas.1700830114>, 2017.
- Rönkkö, T., and Timonen, H.: Overview of Sources and Characteristics of Nanoparticles in Urban Traffic-Influenced Areas, *J. Alzheimer's Dis.*, 72(1), 15–28, <https://doi.org/10.3233/JAD-190170>, 2019.
- 780 Seinfeld, J.H. and Pandis, S.N.: *Atmospheric chemistry and physics: from air pollution to climate change*. John Wiley & Sons, 2016.
- Sofiev, M., Vira, J., Kouznetsov, R., Prank, M., Soares, J., and Genikhovich, E.: Construction of the SILAM Eulerian atmospheric dispersion model based on the advection algorithm of Michael Galperin, *Geosci. Model Dev.*, 8(11), 3497–3522, <https://doi.org/10.5194/gmd-8-3497-2015>, 2015.
- 785 Sofowote, U. M., Healy, R. M., Su, Y., Debosz, J., Noble, M., Munoz, A., Jeong, C. H., Wang, J. M., Hilker, N., Evans, G. J., and Hopke, P. K.: Understanding the PM<sub>2.5</sub> imbalance between a far and near-road location: Results of high temporal frequency source apportionment and parameterization of black carbon, *Atmos. Environ.*, 173, 277–288, <https://doi.org/10.1016/j.atmosenv.2017.10.063>, 2018.
- 790 Tezel-Oguz, M. N., Marasli, M., Sari, D., Ozkurt, N., and Keskin, S. S: Investigation of simultaneous effects of noise barriers on near-road noise and air pollutants, *Sci. Total Environ.*, 892, <https://doi.org/10.1016/j.scitotenv.2023.164754>, 2023.

- Thoma, E. D., Shores, R. C., Isakov, V., and Richard, W. B.: Characterization of near-road pollutant gradients using path-integrated optical remote sensing, In *J Air Waste Manag. Assoc.*, 58(7), 879–890), <https://doi.org/10.3155/1047-3289.58.7.879>, 2008.
- 795 Vouitsis, I., Portugal, J., Kontses, A., Karlsson, H. L., Faria, M., Elihn, K., Juárez-Facio, A. T., Amato, F., Piña, B., and Samaras, Z.: (2023). Transport-related airborne nanoparticles: Sources, different aerosol modes, and their toxicity, *Atmos. Environ.*, 301, <https://doi.org/10.1016/j.atmosenv.2023.119698>, 2023.
- Wlasits, P. J., Enroth, J., Vanhanen, J., Pajunoja, A., Grothe, H., Winkler, P. M., & Stolzenburg, D.: Reduced particle composition dependence in condensation particle counters. *Aerosol Research*, 2(1), 199–206. [https://doi.org/10.5194/ar-2-](https://doi.org/10.5194/ar-2-199-2024)
- 800 199-2024, 2024.
- WHO, WHO global air quality guidelines. *Coastal And Estuarine Processes*, 1–360., 2021.
- Zheng, T., Peng, Z. R., He, H. Di, Zhang, S., and Wu, Y.: Horizontal profiles of size-segregated particle number concentration and black carbon beside a major roadway, *Atmos. Environ.*, 16, <https://doi.org/10.1016/j.aeaoa.2022.100187>, 2022.